Research Paper

THEMED ISSUE: The Tectonic Evolution of the Basin and Range Province: A Themed Issue in Honor of Ernie Anderson

GEOSPHERE

GEOSPHERE

https://doi.org/10.1130/GES02482.1

11 figures; 3 tables; 1 set of supplemental files

CORRESPONDENCE: sean.p.long@wsu.edu

CITATION: Long, S.P., Lee, J., and Blackford, N.R., 2022, The low-angle breakaway system for the Northern Snake Range décollement in the Schell Creek and Duck Creek Ranges, eastern Nevada, USA: Implications for displacement magnitude: Geosphere, https://doi.org/10.1130/GES02482.1.

Science Editor: David E. Fastovsky
Associate Editor: Andrew V. Zuza

Received 7 September 2021
Revision received 7 January 2022
Accepted 1 March 2022

Published online 12 May 2022

The low-angle breakaway system for the Northern Snake Range décollement in the Schell Creek and Duck Creek Ranges, eastern Nevada, USA: Implications for displacement magnitude

Sean P. Long[1], Jeffrey Lee[2], and Nolan R. Blackford[1]

[1]School of the Environment, Washington State University, Pullman, Washington 99164, USA
[2]Department of Geophysics, Colorado School of Mines, Golden, Colorado 80401, USA

ABSTRACT

Documenting the kinematics of detachment faults can provide fundamental insights into the ways in which the lithosphere evolves during high-magnitude extension. Although it has been investigated for 70 yr, the displacement magnitude on the Northern Snake Range décollement in eastern Nevada remains vigorously debated, with published estimates ranging between <10 and 60 km. To provide constraints on displacement on the Northern Snake Range décollement, we present retrodeformed cross sections across the west-adjacent Schell Creek and Duck Creek Ranges, which expose a system of low-angle faults that have previously been mapped as thrust faults. We reinterpret this fault system as the extensional Schell Creek Range detachment system, which is a stacked series of top-down-to-the-ESE brittle normal faults with 5°–10° stratigraphic cutoff angles that carry 0.1–0.5-km-thick sheets that are up to 8–13 km long. The western portion of the Schell Creek Range detachment system accomplished ~5 km of structural attenuation and is folded across an antiformal culmination that progressively grew during extension. Restoration using an Eocene unconformity as a paleohorizontal marker indicates that faults of the Schell Creek Range detachment system were active at ~5°–10°E dips. The Schell Creek Range detachment system accommodated 36 km of displacement via repeated excision, which is bracketed between ca. 36.5 and 26.1 Ma by published geochronology. Based on their spatial proximity, compatible displacement sense, overlapping deformation timing, and the similar stratigraphic levels to which these faults root, we propose that the Schell Creek Range detachment system represents the western breakaway system for the Northern Snake Range décollement. Debates over the pre-extensional geometry of the Northern Snake Range décollement hinder an accurate cumulative extension estimate, but our reconstruction shows that the Schell Creek Range detachment system fed at least 36 km of displacement eastward into the Northern Snake Range décollement.

Sean Long https://orcid.org/0000-0001-6548-9394

INTRODUCTION

Metamorphic core complexes represent some of the most striking end products of high-magnitude extensional tectonism, and deciphering their geometry and dynamics can provide fundamental insights into the ways in which the lithosphere evolves thermally, mechanically, and temporally during extension (e.g., Crittenden et al., 1980; Buck, 1991; Whitney et al., 2013; Platt et al., 2015). In the Basin and Range Province in the western United States (Fig. 1A), a series of Cenozoic metamorphic core complexes have deformed the Cordilleran orogenic belt (e.g., Dickinson, 2002, 2006) and are interpreted to have accommodated the extensional collapse of thickened orogenic crust during and after the final stages of subduction of the Farallon oceanic plate (e.g., Coney and Harms, 1984; Dewey, 1988; Lister and Davis, 1989; Allmendinger, 1992; Dilek and Moores, 1999; Sonder and Jones, 1999). The Northern Snake Range metamorphic core complex in east-central Nevada (Fig. 1A) is a classic example that has been extensively studied over the past 70 yr (e.g., Hazzard et al., 1953; Misch and Hazzard, 1962; Coney, 1974; Miller et al., 1983; Bartley and Wernicke, 1984; Lee et al., 1987; Lee and Sutter, 1991; Lewis et al., 1999; Cooper et al., 2010; Wrobel et al., 2021). However, considerable debate remains about the geometric and kinematic evolution of the Northern Snake Range. One prominent debate focuses on the magnitude of displacement on the Northern Snake Range décollement, a top-down-to-the-ESE, low-angle detachment fault that separates brittlely extended rocks in its hanging wall from ductilely stretched rocks in its footwall (e.g., Miller et al., 1983; Lee et al., 1987). Due to the complexity of polyphase hanging-wall normal faulting and the lack of any offset markers that can be restored across the Northern Snake Range décollement, this question has confounded researchers for the past 40 yr, and it has yielded interpretations that range from <10 km of differential displacement (Miller et al., 1983) to as much as 60 km (Bartley and Wernicke, 1984). Because the Northern Snake Range is a classic locality for the development of widely applied models of core complex dynamics (e.g., Wernicke, 1981; Miller et al., 1983; Lister et al., 1986; Gans, 1987; Lister and Davis, 1989), quantifying the displacement magnitude on the Northern Snake

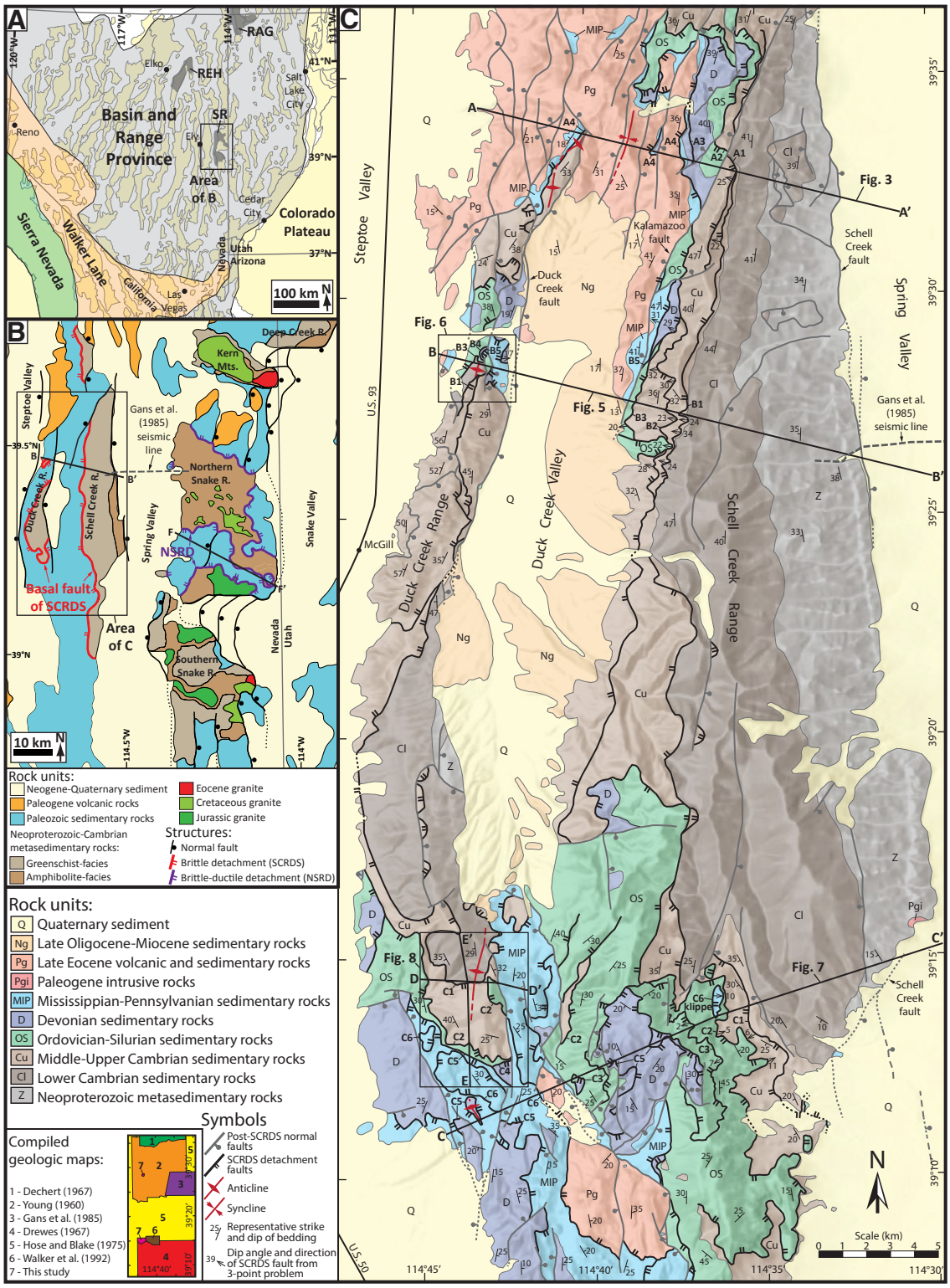

Figure 1. (A) Map of the Basin and Range Province in Nevada and western Utah (modified from Long, 2019), showing the locations of metamorphic core complexes (SR—Snake Range; REH—Ruby–East Humboldt; RAG—Raft River–Albion–Grouse Creek). (B) Generalized geologic map of the Duck Creek, Schell Creek, Northern Snake, and southern Snake Ranges (modified from Lee et al., 2017). The map pattern of the basal fault of the Schell Creek Range detachment system (SCRDS) is outlined in red, and the map pattern of the Northern Snake Range décollement (NSRD) is outlined in purple. R.—Range, Mts.—Mountains. (C) Geologic map of the Schell Creek and Duck Creek Ranges, compiled from the mapping of Young (1960), Dechert (1967), Drewes (1967), Hose and Blake (1976), Gans et al. (1985), Walker et al. (1992), and this study. The locations of the lines of section for A-A′, B-B′, C-C′, D-D′, and E-E′ are shown, as well as the map areas for Figures 6 and 8. Individual Schell Creek Range detachment faults discussed in the text (A1–A4, B1–B5, C1–C6) are labeled along with strike and dip symbols defining representative bedding attitudes (from Young, 1960; Drewes, 1967) and attitudes of Schell Creek Range detachment faults determined from three-point problems (supporting data in Table S3 [see text footnote 1]).

Range décollement has implications not just for elucidating the kinematics of this classic Cordilleran core complex, but for understanding the structural evolution of core complexes in general.

In this study, we approached this problem by investigating the Schell Creek and Duck Creek Ranges, which are the adjacent mountain ranges to the west of the Northern Snake Range (Fig. 1B). Early mapping in these ranges by Young (1960), Dechert (1967), and Drewes (1967) revealed a system of NNE-striking, low-dip-angle, low-stratigraphic-cutoff-angle brittle faults, which were originally interpreted as thrust faults. Based on analysis of the field relationships presented on these early maps, as well as our new mapping of exposures of several of these faults, we reexamined this interpretation by constructing three retrodeformable cross sections across the Schell Creek and Duck Creek Ranges. We propose that these low-angle faults define a top-down-to-the-ESE, normal-sense brittle detachment fault system that fed displacement eastward into the Northern Snake Range décollement, and therefore they represent the breakaway zone for a linked extensional fault system that spans the width of the Duck Creek, Schell Creek, and Northern Snake Ranges. We then explored the implications for the magnitude of displacement on the Northern Snake Range décollement by combining one of our cross sections with the seismic reflection data of Gans et al. (1985) and a new cross section across the Northern Snake Range that integrates the finite strain data of Lee et al. (1987). Finally, we examined the implications of our results for regional extension in eastern Nevada, and for models of the style of hanging-wall deformation above low-angle detachment fault systems.

REGIONAL TECTONIC SETTING

Eastern Nevada was the site of deposition of an ~15-km-thick section of Neoproterozoic to Mesozoic shallow-marine sedimentary rocks on the west-facing North American passive continental margin (e.g., Stewart and Poole, 1974; Stewart, 1980). During the Jurassic, the establishment of an Andean-style subduction zone on the western North American margin initiated construction of the Cordilleran orogen, which continued until the Paleogene (e.g., Allmendinger, 1992; DeCelles, 2004; Dickinson, 2004; Yonkee and Weil, 2015). Over the duration of Cordilleran orogenesis, eastern Nevada was situated within a broad retroarc region in the hinterland of the Sevier fold-and-thrust belt in western Utah (e.g., Armstrong, 1968, 1972; Gans and Miller, 1983; Long, 2012). During orogenesis, eastern Nevada experienced episodes of granitic magmatism and associated metamorphism during the Jurassic and Late Cretaceous (e.g., Miller et al., 1988; Barton, 1990; Wells and Hoisch, 2008; Long and Soignard, 2016). Neoproterozoic to Cambrian sedimentary rocks exposed in the Snake and Schell Creek Ranges record greenschist- to amphibolite-facies metamorphism, with peak metamorphic conditions interpreted to have been attained during a Late Cretaceous magmatic episode (Fig. 1B; e.g., Miller and Gans, 1989; Cooper et al., 2010; Blackford et al., 2022). By the late stages of Cordilleran thickening in the Late Cretaceous–early Paleogene, eastern Nevada is interpreted to have been a high-elevation plateau underlain by ~50–60-km-thick crust (e.g., Coney and Harms, 1984; Cassel et al., 2014; Snell et al., 2014; Chapman et al., 2015; Long, 2019).

Following Cordilleran contraction, eastern Nevada underwent a protracted transition to an extensional regime. Eocene–Oligocene extension is documented in several areas of eastern Nevada (e.g., Gans and Miller, 1983; Gans et al., 1989, 2001; Druschke et al., 2009; Long et al., 2018) and broadly overlapped in time with the Great Basin ignimbrite flare-up, a NE-to-SW sweep of silicic volcanism that is interpreted to be the consequence of post-Laramide slab rollback (e.g., Humphreys, 1995; Dickinson, 2002; Smith et al., 2014). Extension within metamorphic core complexes in eastern Nevada, including the Northern Snake Range and Ruby–East Humboldt core complexes (Fig. 1A), began during the Eocene–Oligocene (e.g., Gans et al., 1989; Lee and Sutter, 1991; Lee, 1995; Dickinson, 2002; Henry et al., 2011; Lee et al., 2017). The widespread upper-crustal normal faulting that formed the Basin and Range Province initiated during the Miocene (e.g., Dickinson, 2002, 2006; Colgan and Henry, 2009).

STRATIGRAPHY OF THE SCHELL CREEK AND DUCK CREEK RANGES

Bedrock exposed in the Schell Creek and Duck Creek Ranges consists of an ~10-km-thick, conformable section of Neoproterozoic to Paleozoic sedimentary rocks, which is unconformably overlain by up to ~1 km of Paleogene sedimentary and volcanic rocks (Fig. 2; Young, 1960; Dechert, 1967; Drewes, 1967; Hose and Blake, 1976; Gans et al., 1985). Readers are referred to Young (1960) for lithologic descriptions, and details on unit thicknesses used in our study are included in the Supplemental Material[1] (Text S1 and Table S1). The Neoproterozoic section (our lumped unit Z) consists of at least 3.2 km of dominantly greenschist-facies metasedimentary clastic rocks of the McCoy Creek Group, which Gans et al. (1985) divided into multiple subunits (Fig. 2). Metamorphic grade increases stratigraphically downward in the McCoy Creek Group, with pelitic lithologies progressing from argillite to phyllite to schist (Miller et al., 1988; Miller and Gans, 1989). The overlying 6.6-km-thick Paleozoic section lacks evidence for metamorphism (Young, 1960; Miller and Gans, 1989). The base of this section consists of 1.3 km of Lower Cambrian clastic rocks (our lumped unit Cl). The overlying Middle Cambrian to Pennsylvanian section is dominated by carbonates, including 1.9 km of Middle–Upper Cambrian limestone (our lumped unit Cu), 1.8 km of Ordovician–Silurian limestone and dolomite (our lumped unit OS), 0.9 km of Devonian dolomite (our lumped unit D), and 0.7 km of Mississippian and Pennsylvanian shale and limestone (our lumped unit MIP).

[1]Supplemental Material. Includes supporting data for rock unit thicknesses, tables that list geometric constraints for faults, annotated geologic maps and Google Earth images, and field photographs of fault zone rocks and field relationships. Please visit https://doi.org/10.1130/GEOS.S.19394168 to access the supplemental material, and contact editing@geosociety.org with any questions. To view Figure 5 at full size, please visit https://doi.org/10.1130/GEOS.S.19394201 or access the full-text article on www.gsapubs.org.

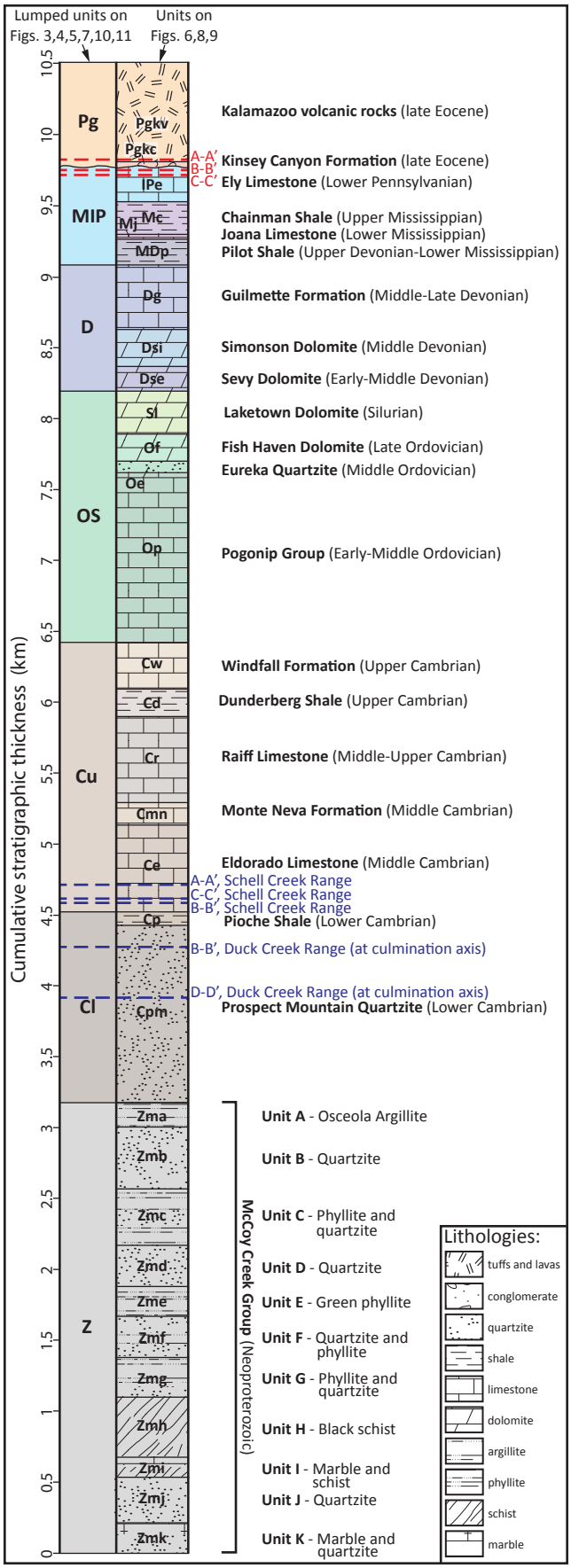

Figure 2. Composite stratigraphic column for the Schell Creek and Duck Creek Ranges at the latitude of sections A-A′ and B-B′. The right side of the column shows formation-level divisions of Paleozoic rock units from Young (1960) and subdivided units of the Neoproterozoic McCoy Creek Group from Gans et al. (1985). The left side of the column shows the lumped unit scheme shown on Figures 3, 4, 5, 7, 10, and 11 (Z—Neoproterozoic, Cl—Lower Cambrian, Cu—Middle–Upper Cambrian, OS—Ordovician–Silurian, D—Devonian, MIP—Mississippian–Pennsylvanian, Pg—Paleogene). Unit thicknesses were either constrained on our cross sections or were taken from Young (1960); see Text S1 and Table S1 for details (text footnote 1). Red dashed lines show the highest hanging-wall stratigraphic level of the structurally highest fault of the Schell Creek Range detachment system on each cross section, and blue dashed lines show the lowest footwall stratigraphic level of the structurally lowest fault of the Schell Creek Range detachment system.

Paleozoic rocks are unconformably overlain by Paleogene rocks (our lumped unit Pg), which include the Kinsey Canyon Formation and the overlying Kalamazoo volcanic rocks (Fig. 2; Young, 1960). The unconformity at the base of the Paleogene section exhibits minimal angular discordance (typically <5°) with underlying Paleozoic rocks and most often lies within the Pennsylvanian section (Young, 1960; Drewes, 1967; Gans and Miller, 1983; Gans et al., 1985). However, in the northern part of the Schell Creek Range, the unconformity also locally lies within Mississippian rocks, and in one locality, it lies within the top ~20 m of the Devonian section (Young, 1960), corresponding to a total pre-unconformity structural relief of 0.7 km. The Kinsey Canyon Formation, which consists of up to 100 m of tuffaceous conglomerate, sandstone, and lacustrine limestone (Young, 1960), has been correlated with the Paleocene–Eocene Sheep Pass Formation that is mapped in adjacent regions of eastern Nevada (Fouch et al., 1979). U-Pb ages of detrital zircons and $^{40}Ar/^{39}Ar$ sanidine dating of tuffaceous horizons bracket deposition of the Kinsey Canyon Formation between ca. 36.5 and 35.2 Ma (late Eocene; Druschke et al., 2009, 2011). The overlying Kalamazoo volcanic rocks consist of felsic tuffs and dacitic lavas that are up to 1.1 km thick (Young, 1960; Gans et al., 1989; Hagstrum and Gans, 1989), and $^{40}Ar/^{39}Ar$ sanidine ages collected from tuff samples in the Schell Creek Range bracket their emplacement between ca. 36.1 and 35.2 Ma (late Eocene; Druschke et al., 2009).

In Duck Creek Valley, a modern topographic basin that separates the Duck Creek Range from the central Schell Creek Range (Fig. 1C), conglomerate of the North Creek Formation overlies Paleozoic and Paleogene rocks across an angular unconformity (Young, 1960; Anderson, 1983). The North Creek Formation is interpreted to represent synextensional sediments deposited within a west-tilted half graben that occupies present-day Duck Creek Valley (Anderson, 1983; Gans et al., 1985). Anderson (1983) obtained a 27.4 ± 1.3 Ma zircon fission-track age from a tuffaceous horizon 150 m above the base of the North Creek Formation, indicating that deposition had begun by the late Oligocene. There are no timing constraints available on the cessation of deposition of the North Creek Formation; however, given its thickness and the age range of deposition within other half grabens in the region (e.g., Gans et al., 1985), we speculate that deposition likely continued into the Miocene.

STRUCTURAL FRAMEWORK OF THE SCHELL CREEK AND DUCK CREEK RANGES: SUMMARY OF PUBLISHED WORK

The Schell Creek and Duck Creek Ranges are deformed by a system of low-dip-angle (typically ~10–25°W), low-stratigraphic-cutoff-angle (typically ~5°–10°, cutting down section to the east) brittle faults that consistently place younger rocks over older rocks, which we term here the Schell Creek Range detachment system (Fig. 1C). Young (1960) was the first to describe the Schell Creek Range detachment system; he mapped them as thrust faults and documented several important field relationships, including the following: (1) each fault exhibits low cutoff angles and omits strata; (2) structurally higher faults cut structurally lower faults; (3) the structurally highest fault cuts the Kalamazoo volcanic rocks; (4) two of the structurally highest faults exhibit drag folds that define a top-to-the-ESE sense of motion; and (5) all faults exhibit localized zones of brecciation. Young (1960) explored several hypotheses for the origin of the Schell Creek Range detachment system, including thrust faulting or gravity sliding within the limb of an anticline, as well as the possibility of a regional thrust décollement, which had recently been proposed for the Northern Snake Range to the east (Hazzard et al., 1953; Hazzard and Turner, 1957; Misch, 1957). Young (1960) concluded that no individual explanation was convincing for the origin of the Schell Creek Range detachment system. His mapping and structural observations formed the foundation of our study.

Following on Young's work, Drewes (1967) and Dechert (1967) mapped similar systems of low-cutoff-angle "thrust faults" in the southern and northern Schell Creek Range, respectively, thereby extending the N-S spatial extent of the Schell Creek Range detachment system to at least ~85 km (Figs. 1B–1C). Anderson (1983, p. 23) presented a brief structural analysis that was primarily focused on the development of the Duck Creek Valley half graben and was the first to state that the Schell Creek Range detachment system likely represented "an episode of major attenuation faulting that probably reflects large-magnitude crustal extension."

In the 1970s and 1980s, significant progress was made in documenting the structural framework of the Northern Snake Range to the east (Fig. 1B), including the interpretation of the Northern Snake Range décollement as a top-down-to-the-ESE extensional detachment fault that separates ductilely stretched and thinned Neoproterozoic–Lower Cambrian clastic rocks in its footwall from brittlely extended Middle Cambrian–Permian carbonates in its hanging wall (Coney, 1974; Gans and Miller, 1983; Miller et al., 1983; Bartley and Wernicke, 1984; Gans et al., 1985; Lee et al., 1987). Gans et al. (1985) was the first to interpret that extension in the Northern Snake Range and Schell Creek/Duck Creek Ranges was genetically related. Using an interpreted seismic reflection profile across Spring Valley, they presented a cross section that spanned from the Duck Creek Range to the western flank of the Northern Snake Range, and they interpreted that the Schell Creek Range detachment system represents the westernmost faults that fed displacement into the Northern Snake Range décollement. Gans et al. (1985) interpreted the faults of the Schell Creek Range detachment system as top-down-to-the-E, domino-style normal faults that initiated at ~60° dip angles, which sole downward into the Northern Snake Range décollement at the top of the Lower Cambrian section (their fig. 4).

Blackford et al. (2022) presented a retrodeformed cross section through the Schell Creek and Duck Creek Ranges, supported by the mapping of Young (1960) and Gans et al. (1985). Their study was the first to document that faults of the Schell Creek Range detachment system have low stratigraphic cutoff angles across all exposed structural levels, which requires large-magnitude (~32 km) cumulative top-down-to-the-E displacement. However, as their paper was focused on understanding upper-crustal thermal conditions, they did not explore the implications of this displacement for the Northern Snake Range décollement, and they did not attempt to kinematically relate the extension in the Schell Creek Range to the Northern Snake Range.

GEOMETRY AND DISPLACEMENT MAGNITUDE OF THE SCHELL CREEK RANGE DETACHMENT SYSTEM FROM CROSS SECTIONS

To illustrate the geometry and quantify the magnitude of extension across the Duck Creek and Schell Creek Ranges, we utilized published geologic mapping (Young, 1960; Drewes, 1967; Gans et al., 1985) combined with our new mapping of areas of the Duck Creek Range to construct three retrodeformable cross sections (A-A′, B-B′, C-C′). (To provide additional context on the level of detail of the geologic mapping that supported the cross sections, the breccia zones developed along faults of the Schell Creek Range detachment system, and the low stratigraphic cutoff angles and crosscutting relationships exhibited by the faults of the Schell Creek Range detachment system, we include geologic maps, field photographs, and annotated Google Earth images in Figs. S1–S4 in the supplemental material [see footnote 1].) The lines of section are oriented normal to the average strike direction of Schell Creek Range detachment system faults, which is 015° at the latitudes of cross-sections A-A′ and B-B′ and 340° at the latitude of cross-section C-C′ (Fig. 1C). The cross sections are supported by apparent dips of bedding measurements (n = 139 for A-A′, 151 for B-B′, and 138 for C-C′), and they were divided into domains of average, approximately homogeneous apparent dip, with their boundaries modeled as kink surfaces that bisect the interlimb angle (e.g., Suppe, 1983). Due to the scale of the cross sections, several post–detachment system normal faults with <100 m of displacement were not included, and areas where the Schell Creek Range detachment system exhibits multiple fault planes that are separated by <100 m of structural distance were simplified as one fault plane. Estimates of the average dip angles of faults were determined using three-point problems (n = 45) and the interactions of fault traces with topography along the line of section (Tables 1 and 2; supporting data in Tables S2–S4). Combining fault dip angles with the defined domains of average apparent dip allowed us to calculate average stratigraphic cutoff angles for segments of Schell Creek Range detachment system faults (Table 2). The thicknesses of our lumped rock units (shown in the left-hand column of Fig. 2) were either constrained along the cross sections or were taken from Young (1960) (see Text S1 and Table S1 for details). Angular relationships and contacts offset across faults were drafted

TABLE 1. DIP ANGLE CONSTRAINTS AND DISPLACEMENT ESTIMATES FOR POST–SCHELL CREEK RANGE DETACHMENT SYSTEM NORMAL FAULTS

Cross section	Fault (listed from east to west for each cross section)	Dip angle at modern surface, proximal to trace	Displacement (m)	Motion sense on cross section
A-A′	E-dipping Schell Creek fault (NgQ over Z)	Not constrained; 45°E dip from B-B′ shown	Not constrained	Top-down-to-east
A-A′	W-dipping Z over Z fault	78°W (three-point problem)	365	Top-down-to-west
A-A′	E-dipping Cl over Z fault	24°E (average of two three-point problems)	915	Top-down-to-east
A-A′	E-dipping Cl over Z fault	34°E (three-point problem)	275	Top-down-to-east
A-A′	W-dipping Kalamazoo fault (OS over Cu)	81°W (three-point problem)	670	Top-down-to-west
A-A′	NW-dipping D over D fault	72°NW (three-point problem)	625	Top-down-to-west
A-A′	E-dipping Pg over D fault	60°E (approximated)	685	Top-down-to-east
A-A′	E-dipping Pg over Pg fault	82°E (three-point problem)	335	Top-down-to-east
A-A′	W-dipping Pg over Pg fault	55°W (three-point problem)	290	Top-down-to-west
A-A′	E-dipping Duck Creek fault (Pg over Cu)	52°E (three-point problem)	380	Top-down-to-east
A-A′	W-dipping listric fault array (6 faults)	71°W (average of six three-point problems)	100–455 range	Top-down-to-west
B-B′	E-dipping Schell Creek fault (NgQ over Z)	45°E (Gans et al., 1985, seismic cross section)	10,450	Top-down-to-east
B-B′	E-dipping Cl over Cl fault	46°E (three-point problem)	730	Top-down-to-east
B-B′	W-dipping Kalamazoo fault (MIP over OS)	83°W (three-point problem)	790	Top-down-to-west
B-B′	E-dipping Duck Creek fault (NgQ over MIP)	52°E (three-point problem projected from A-A′)	1175	Top-down-to-east
B-B′	E-dipping MIP over D fault	60°E (approximated)	120	Top-down-to-east
B-B′	E-dipping OS over Cl fault	39°E (three-point problem)	105	Top-down-to-east
C-C′	E-dipping Schell Creek fault (NgQ over Z)	Not constrained; 45°E dip from B-B′ shown	Not constrained	Top-down-to-east
C-C′	W-dipping fault (Cu over Cl)	72°W (three-point problem)	170	Top-down-to-west
C-C′	E-dipping fault (D over OS)	42°E (three-point problem)	130	Top-down-to-east
C-C′	SW-dipping fault (MIP over OS)	58°SW (three-point problem)	670	Top-down-to-west
C-C′	SW-dipping fault (Pg over MIP)	58°SW (approximated from adjacent fault to E)	760	Top-down-to-west
C-C′	W-dipping fault (MIP over MIP)	58°W (approximated from faults to E)	170	Top-down-to-west
C-C′	W-dipping fault (MIP over MIP)	58°W (approximated from faults to E)	505	Top-down-to-west
C-C′	NE-dipping fault (MIP over D)	42°NE (approximated from adjacent fault to W)	260	Top-down-to-east
C-C′	NE-dipping fault (MIP over MIP)	42°NE (three-point problem)	135	Top-down-to-east

Note: See Table S2 for supporting data (see text footnote 1). A guide to rock unit abbreviations is shown on Figure 2.

TABLE 2. GEOMETRIC CONSTRAINTS, DISPLACEMENT ESTIMATES, AND CROSSCUTTING RELATIONSHIPS FOR SCHELL CREEK RANGE DETACHMENT SYSTEM FAULTS

Fault number	Dip angle at modern surface, proximal to trace	Stratigraphic cutoff angle at modern surface, proximal to trace	Displacement (km)	Stratigraphic omission at trace (km)	Structural thickness of hanging-wall sheet (km)	Crosscutting relationships
Cross-section A-A′						
A4	33°W** (between SCR and DCR) 15°W** (DCR)	4° (hanging wall and footwall; between eastern two traces) 2° (MIP), –2° (Pg) (hanging wall; between western two traces) 4° (MIP), 2° (Pg) (hanging wall; at and west of DCR trace) 11° (footwall; at DCR trace; approximate maximum from A1)	2.9	0.23 (eastern trace) 3.65 (DCR trace)	0.70 minimum preserved	Cuts A3, A2, A1 (required) Cuts base of Pg section (observed)
A3	27°W approximated based on A1 (SCR)	11° approximate maximum (hanging wall and footwall)	0.2	0.05	0.34 (at SCR trace) Cut out westward before DCR	
A2	27°W approximated based on A1 (SCR)	11° approximate maximum (hanging wall and footwall)	12.3	2.43	0.76 (SCR) Cut out westward before DCR	
A1	27°W minimum** (SCR)	11° maximum (hanging wall and footwall)**	1.4	0.24	0.43 (SCR) Cut out westward before DCR	
Cross-section B-B′						
B5	27°W* (SCR) 17°E* (eastern DCR)	8° (hanging wall and footwall, SCR) 5° (hanging wall, eastern DCR)	9.3	2.27 (SCR) 1.35 (at DCR culmination axis)	1.11 minimum preserved (SCR) 0.15 minimum preserved (DCR)	Cuts B4 (required, between DCR and SCR)
B4	21°E** (eastern DCR)	6° (hanging wall, eastern DCR)	6.5	0.28 (at DCR culmination axis)	0.06 (DCR)	Cuts B3 in DCR (observed)
B3	27°W* (SCR) 26°W** (western DCR)	8° (hanging wall and footwall, SCR) 10° (footwall, western DCR)	5.1	0.58 (SCR) 3.12 (at DCR culmination axis)	0.15 (SCR) 0.07 (at DCR culmination axis)	Cuts B2 (observed, SCR and DCR) Merges with B1 (observed, DCR)
B2	27°W* (western SCR)	8° (hanging wall and footwall, SCR)	0.6	0.05 (SCR)	0.34 (SCR) Cut out east of DCR culmination axis	Merges with B1 (observed, SCR)
B1	27°W*,** (SCR) 5°E** (DCR crest) 17°W** (western DCR)	8° (hanging wall and footwall, SCR) 10° (footwall, western DCR) –2° (footwall, between SCR and DCR)	14.5	0.82 (SCR) 0.58 (at DCR culmination axis)	0.09 (SCR) 0.03 (at DCR culmination axis)	
Cross-section C-C′						
C6	5-17°E*,** (klippe in SCR) 23°E** (east of culmination axis, DCR) 12°W** (west of culmination axis, DCR)	4° (hanging wall, between DCR and SCR klippe) 0–2° (hanging wall, DCR) 4° (footwall, DCR)	7.5	3.05 (klippe in SCR) 0.06 (western DCR)	0.02 minimum preserved (SCR klippe) 0.55 minimum preserved (DCR)	Cuts C5 and C3 (required, SCR) Cuts C5 (observed, DCR) Cuts and merges with C1 (observed, DCR) Cuts base of Pg section (observed, SCR)
C5	0–3°W** (SCR crest zone) 24°E** (east of culmination axis, DCR) 12°W** (west of culmination axis, DCR)	4° maximum (hanging wall) 3–4° maximum (footwall)	4.5	0.64 (SCR crest) 0.34 (western DCR)	0.41 (DCR and SCR)	Cuts C4 (observed, DCR) Cuts or merges with C3 (observed, SCR)
C4	Trace not exposed on section line	4° approximate maximum (hanging wall and footwall)	4.3	0.29 (eastern DCR)	0.14 (approximate; western DCR)	Cuts C3 (required, DCR)
C3	5°W*,** (SCR crest) 14°W** (western SCR)	3° maximum (hanging wall) 6° (footwall)	10.9	1.12 (central SCR) 1.10 (eastern DCR)	0.14 (central SCR) Cut out westward in eastern DCR	Cuts C2 (observed, SCR)
C2	8°E*,** (eastern SCR)	6° maximum (hanging wall) 7° maximum (footwall)	11.9	0.94 maximum (eastern SCR) 1.10 maximum (western DCR)	0.27 (eastern SCR) 0.06 (western DCR)	Merges with C1 (observed, SCR)
C1	8°W*,** (eastern SCR)	0° (footwall, SCR and DCR) 7° maximum (hanging wall, SCR and DCR)	12.8	0 minimum (eastern SCR) 1.55 maximum (western DCR)	0.25 (eastern SCR)	

Note: Data reported with one asterisk are constrained by three-point problems, and data reported with two asterisks are constrained by cross-section geometry; see Table S3 for supporting data (see text footnote 1). See Figure 2 for a guide to rock unit abbreviations. SCR—Schell Creek Range; DCR—Duck Creek Range.

so that they matched up when displacement was retrodeformed. Each cross section underwent two phases of retrodeformation: The first restored displacement and tilting accomplished by post–Schell Creek Range detachment system normal faults, and the second restored the cumulative displacement accommodated by the Schell Creek Range detachment system. We made drafting decisions aimed at maximizing stratigraphic cutoff angles on detachment faults, in order to minimize displacement. Positive cutoff angles represent faults cutting down section toward the east, and negative cutoff angles represent faults cutting down section toward the west.

Faults of the Schell Creek Range detachment system were grouped genetically based on their common geometry and style (low dip angles, low stratigraphic cutoff angles, and consistent omission of stratigraphy) and their kinematics in cross section, which show that they consistently offset stratigraphic contacts toward the east and cut down section toward the east (exceptions, such as flats, are discussed below). Due to differences in the total number of faults observed on each cross section, we did not attempt to correlate individual detachment faults along strike. Instead, we numbered the Schell Creek Range detachment system faults individually on each cross section, from structurally low to high.

Cross-Section A-A′

Cross-section A-A′ (Fig. 3) is supported by the mapping of Young (1960) (Fig. S1A). Multiple post–Schell Creek Range detachment system normal faults are present on A-A′ and exhibit dip angles typically between 50° and 80° and displacement magnitudes on the order of 0.3–0.7 km (Table 1). Due to a lack of information on the subsurface geology in Spring Valley along cross-section A-A′, we could not document the magnitude of displacement on the range-bounding Schell Creek fault, nor the magnitude of tilting accommodated by post–Schell Creek Range detachment system normal faults. Assuming a westward tilt magnitude of 15°, as constrained on cross-section B-B′ (discussed below), retrodeformation of post–detachment system normal faults yielded 3.3 km of minimum extension (27%; Fig. 3). However, assuming a similar dip (45°E) and displacement magnitude (10.5 km) for the Schell Creek fault as constrained on cross-section B-B′ (discussed below) would yield 11.4 km of post–detachment system extension on A-A′ (93%).

Four separate detachment faults are present along A-A′ (Fig. 1). The structurally lowest detachment fault (A1) is exposed at the crest of the Schell Creek Range, where it omits 0.25 km of the basal portion of unit Cu. Proximal to its trace, A1 is shown at a dip angle of 27°W, which is the minimum dip angle possible without intersecting the modern surface to the west of its trace, which defines a maximum stratigraphic cutoff angle of 11°. The second structurally lowest detachment fault (A2) omits 2.45 km of units Cu and OS, and the third lowest detachment fault (A3) omits 0.05 km of unit D. Robust constraints on the dip angles of detachment faults A2 and A3 were not available, so they are shown at a dip of 27°W proximal to their traces, to match the minimum dip angle and 11° maximum cutoff angle shown for detachment fault A1.

The map trace of the structurally highest detachment fault (A4) is exposed in three separate locations along cross-section A-A′ (Figs. 1 and 3). The eastern two traces place the base of unit Pg over unit MIP, corresponding to omission of 0.25 km of stratigraphy and defining a dip of 33°W and a cutoff angle of 4°. The western trace is exposed in the Duck Creek Range, and it places unit MIP (0.1 km stratigraphically below the basal Paleogene unconformity) over unit Cu, corresponding to omission of 3.65 km of stratigraphy. Although it is possible that there are structurally deeper detachment horizons, A4 is interpreted as the structurally lowest detachment fault in the Duck Creek Range at this latitude, based on an ~1-km-thick continuous section of Cambrian stratigraphy in its footwall that is undisturbed by faulting (Figs. 1 and 3).

The axes of a NNE-trending anticline and a NNE-trending syncline are exposed along cross-section A-A′ (Figs. 1 and 3), and they provide important constraints for interpreting the subsurface geometry of the Schell Creek Range detachment system. The syncline, located east of the Duck Creek Range, is developed within Paleogene rocks, and it has an ~35°W-dipping eastern limb and an ~30°E-dipping western limb. The anticline, developed within unit Cu in the footwall of detachment fault A4 in the Duck Creek Range, has an ~30°E-dipping eastern limb and an ~20°W-dipping western limb. Paleogene rocks in the hanging wall of A4 are not exposed within the hinge zone of the anticline (Fig. 1), but they dip ~30°E on average in its eastern limb and ~17°W on average in its western limb (Fig. 3), indicating that the anticline folds rocks in both the hanging wall and footwall of A4. Therefore, we interpret that A4 is also folded across the anticline. Average apparent dips define ≤4° of angularity across the basal Paleogene unconformity on cross-section A-A′. Given the minimal angularity of the unconformity, the low stratigraphic cutoff angles of all Schell Creek Range detachment system faults, and the lack of exposure of any detachment faults structurally below A4 in the Duck Creek Range, we interpret that faults A1–A4 are also folded in the subsurface across the syncline axis to the east, and that faults A1–A3 must either be cut by, or merge with, fault A4 between their traces in the Schell Creek Range and the trace of fault A4 in the Duck Creek Range (Fig. 3).

Retrodeformation of the Schell Creek Range detachment system on cross-section A-A′ (Fig. 4A) yielded 1.4 km of top-down-to-the-E displacement on A1, 12.3 km on A2, 0.2 km on A3, and 2.9 km on A4, defining a cumulative displacement magnitude of 16.8 km. The cumulative east-west extension accommodated by the Schell Creek Range detachment system on cross-section A-A′ is 16.1 km (Fig. 4A). This is a minimum estimate because the maximum permissible cutoff angles for faults A1–A3 were used, and we interpret that no other detachment faults underlie A4 in the Duck Creek Range.

Cross-Section B-B′

Cross-section B-B′ (Fig. 5) is supported primarily by the mapping of Young (1960) and is supplemented by bedding measurements from Anderson (1983) in Duck Creek Valley and by our mapping in part of the Duck Creek Range

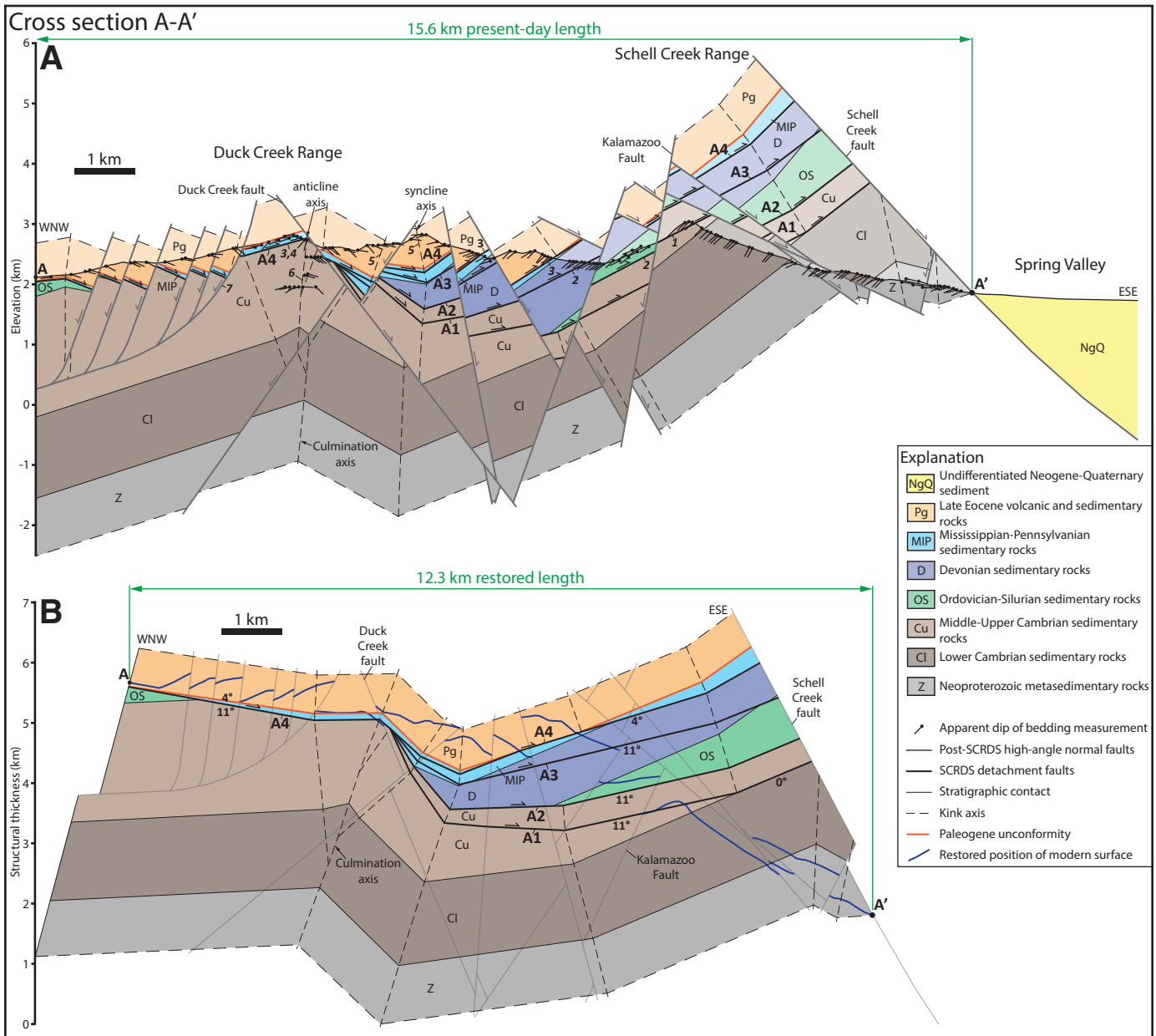

Footnotes:

1 - Detachment A1 is shown at a dip of 27°W, which is the minimum dip required without intersecting the modern surface to the west of its trace. This constrains the maximum possible hanging wall and footwall cutoff angles to 11°. This dip angle is supported by two 3-point problems to the north and south of the section line, which yield 22-25°W dips.

2 - Detachments A2 and A3 are shown at dips of 27°W at and east of their traces, to match the minimum dip angle shown for the underlying detachment A1. This yields 11° hanging wall and footwall stratigraphic cutoff angles, which are likely a maximum for these two faults, and thus minimizes their displacement magnitude.

3 - Three separate traces of detachment faults exposed along the section line are correlated as detachment A4. The eastern two traces define a dip of 33°W and hanging wall and footwall cutoff angles of 4°. Hanging wall stratigraphic levels between the middle and western traces define a cutoff-angle of 2° with respect to MIP and -2° with respect to Pg. At the western trace (in the Duck Creek Range), A4 is shown at a dip of 15°W, which is defined by balancing constraints to the west that limit the maximum hanging wall cutoff angle to 4° with respect to MIP and 2° with respect to Pg. The footwall cutoff angle from the Duck Creek Range westward is approximated at 11°, after the maximum cutoff angle constrained for fault A1 to the east, which minimizes displacement.

4 - A4 is the only SCRDS detachment exposed in the Duck Creek Range at this latitude, and although it is possible that there are structurally deeper detachment horizons, A4 is shown here as the structurally lowest SCRDS fault in the Duck Creek Range. This is supported by a continuous section of ~1.0 km of underlying stratigraphy of unit Cu that is undisturbed by detachment faults for a map distance of ~4 km to the SSW of the section line (Young, 1960). This decision to show A4 as the structurally lowest detachment in the Duck Creek Range minimizes the magnitude of SCRDS extension on this cross section.

5 - Average apparent dips of unit Pg define a syncline with a 34°W-dipping eastern limb, an 8°E-dipping axial zone, and a 30°E-dipping eastern limb. Balancing constraints, and the observations of low stratigraphic cutoff angles on all SCRDS faults at this latitude, and in the rest of the study area, require that faults A1-A4 must also be folded by this syncline, and must be cut by (or merge with) fault A4 between their traces in the Schell Creek Range and the trace of fault A4 in the Duck Creek Range.

6 - At the latitude of the section line, unit Cu dips steeply (~60°) west, but an anticline axis is defined by along-strike projection of E-dipping bedding measurements from Cu 0.3-1.2 km to the S of the section line. A continuation of this anticline axis is observed between 2.3-2.7 km along-strike to the SSW, and these measurements are projected onto the cross section as well, to better define the dip angles of the limbs of the culmination. These measurements are projected to their corresponding stratigraphic level on the cross section. The existence of the anticline axis is further supported by a change in dip of unit Pg (and its basal unconformity) from ~30° average eastward dips in the hanging wall of the Duck Creek fault to ~17° W average westward dips in its footwall . This indicates that the anticline also must fold fault A4.

7 - The six westernmost, steeply W-dipping (average of 71° W), post-SCRDS normal faults are interpreted to represent a listric fault array based on an abrupt westward change in dip direction of unit Pg and its basal unconformity across the easternmost fault, from 17° W in the footwall to a homogeneous dip of 21° E in the hanging wall. The listric fault array is shown with a simple geometry of soling into a W-dipping flat within the western limb of the anticlinal culmination. Alternatively, the change in dip of unit Pg could define a syncline with an axis that is obscured by the easternmost normal fault.

Figure 3. (A) Cross-section A-A′, showing the modern geometry. Schell Creek Range detachment system (SCRDS) faults A1–A4 are labeled, and bold italic numbers are referenced to footnotes. Translucent areas above the modern surface represent eroded rock. (B) Cross-section A-A′ after retrodeformation of displacement on post–Schell Creek Range detachment system normal faults and 15° of post–Schell Creek Range detachment system westward tilting (approximated from the tilting magnitude determined for cross-section B-B′). Stratigraphic cutoff angles are labeled for Schell Creek Range detachment faults.

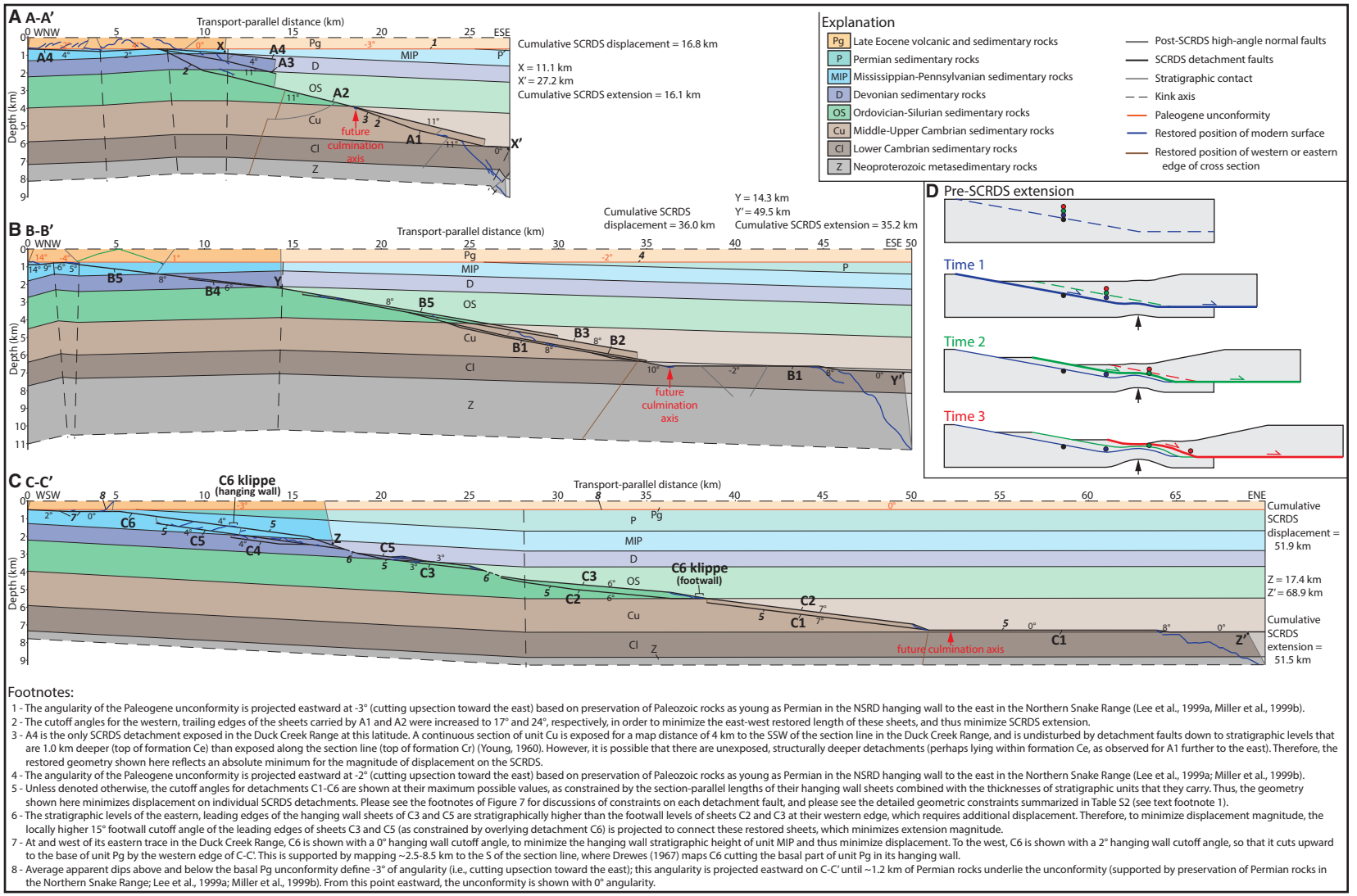

Footnotes:

1 - The angularity of the Paleogene unconformity is projected eastward at -3° (cutting upsection toward the east) based on preservation of Paleozoic rocks as young as Permian in the NSRD hanging wall to the east in the Northern Snake Range (Lee et al., 1999a, Miller et al., 1999b).

2 - The cutoff angles for the western, trailing edges of the sheets carried by A1 and A2 were increased to 17° and 24°, respectively, in order to minimize the east-west restored length of these sheets, and thus minimize SCRDS extension.

3 - A4 is the only SCRDS detachment exposed in the Duck Creek Range at this latitude. A continuous section of unit Cu is exposed for a map distance of 4 km to the SSW of the section line in the Duck Creek Range, and is undisturbed by detachment faults down to stratigraphic levels that are 1.0 km deeper (top of formation Ce) than exposed along the section line (top of formation Cr) (Young, 1960). However, it is possible that there are unexposed, structurally deeper detachments (perhaps lying within formation Ce, as observed for A1 further to the east). Therefore, the restored geometry shown here reflects an absolute minimum for the magnitude of displacement on the SCRDS.

4 - The angularity of the Paleogene unconformity is projected eastward at -2° (cutting upsection toward the east) based on preservation of Paleozoic rocks as young as Permian in the NSRD hanging wall to the east in the Northern Snake Range (Lee et al., 1999a; Miller et al., 1999b).

5 - Unless denoted otherwise, the cutoff angles for detachments C1-C6 are shown at their maximum possible values, as constrained by the section-parallel lengths of their hanging wall sheets combined with the thicknesses of stratigraphic units that they carry. Thus, the geometry shown here minimizes displacement on individual SCRDS detachments. Please see the footnotes of Figure 7 for discussions of constraints on each detachment fault, and please see the detailed geometric constraints summarized in Table S2 (see text footnote 1).

6 - The stratigraphic levels of the eastern, leading edges of the hanging wall sheets of C3 and C5 are stratigraphically higher than the footwall levels of sheets C2 and C3 at their western edge, which requires additional displacement. Therefore, to minimize displacement magnitude, the locally higher 15° footwall cutoff angle of the leading edges of sheets C3 and C5 (as constrained by overlying detachment C6) is projected to connect these restored sheets, which minimizes extension magnitude.

7 - At and west of its eastern trace in the Duck Creek Range, C6 is shown with a 0° hanging wall cutoff angle, to minimize the hanging wall stratigraphic height of unit MIP and thus minimize displacement. To the west, C6 is shown with a 2° hanging wall cutoff angle, so that it cuts upward to the base of unit Pg by the western edge of C-C′. This is supported by mapping ~2.5-8.5 km to the S of the section line, where Drewes (1967) maps C6 cutting the basal part of unit Pg in its hanging wall.

8 - Average apparent dips above and below the basal Pg unconformity define -3° of angularity (i.e., cutting upsection toward the east); this angularity is projected eastward on C-C′ until ~1.2 km of Permian rocks underlie the unconformity (supported by preservation of Permian rocks in the Northern Snake Range; Lee et al., 1999a; Miller et al., 1999b). From this point eastward, the unconformity is shown with 0° angularity.

Figure 4. (A–C) Cross-sections (A) A-A′, (B) B-B′, and (C) C-C′ after retrodeformation of cumulative displacement on Schell Creek Range detachment system (SCRDS) faults. The Paleogene unconformity (orange line) is restored to horizontal. Individual Schell Creek Range detachments, constrained stratigraphic cutoff angles, the angularity of the Paleogene unconformity (orange numbers), and bold italic numbers referenced to footnotes are labeled for each cross section. Translucent areas represent rocks that presently lie to the east of the area of the cross sections shown on Figures 3, 5, and 7. Cumulative displacement on the Schell Creek Range detachment system translated point X above point X′ on A-A′, point Y above point Y′ on B-B′, and point Z above point Z′ on C-C′. The cumulative Schell Creek Range detachment system extension for each cross section was estimated by comparing the transport-parallel distance between the restored positions of points X and X′ (A-A′), Y and Y′ (B-B′), and Z and Z′ (C-C′). (D) Schematic diagrams that illustrate the progressive formation of stacked, detachment-bounded sheets via excision, and the synextensional folding of the Schell Creek Range detachment system across an antiformal culmination. NSRD—Northern Snake Range décollement.

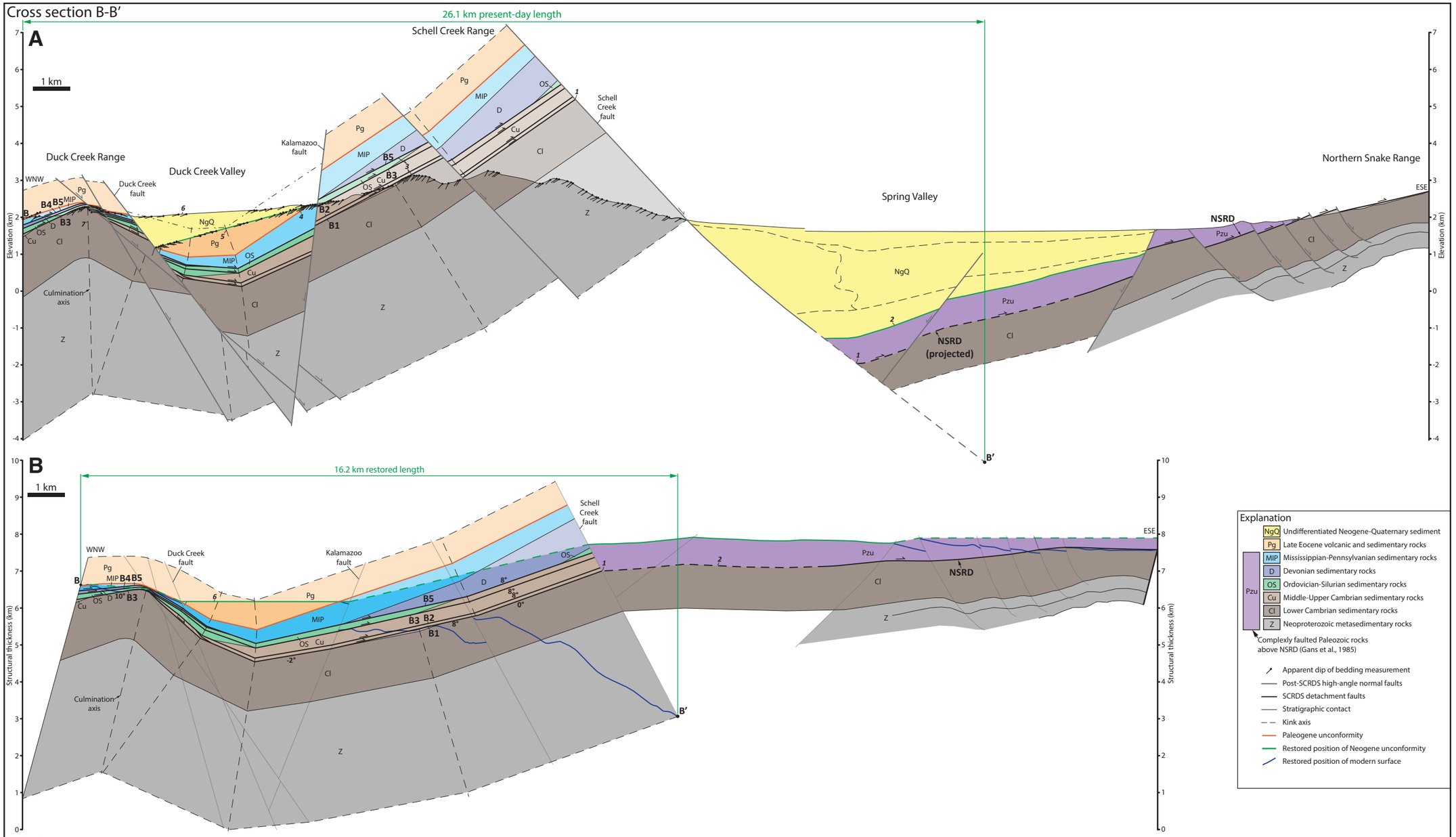

Footnotes:

1 - Displacement on the Schell Creek fault was estimated by projecting the interpreted NSRD horizon from the Gans et al. (1985) seismic cross section 6.3 km westward (at its same structural level) to its intersection with the Schell Creek fault, and then restoring the NSRD to match up with the footwall intersection of SCRDS detachment B1 with the Schell Creek fault. This yielded 10.45 km of top-down-to-east displacement.

2 - The average dip of the basal unconformity of valley fill unit NgQ in Spring Valley on the Gans et al. (1985) seismic cross section is 14.5°W. This, combined with the 16°W average apparent dip of NgQ valley fill in the Duck Creek Valley half-graben, was utilized to retrodeform 15° of average westward tilting for the entire width of the restored cross section.

3 - Detachments B1, B2, B3, and B5 are all shown at a dip of 27°W at and proximal to their traces in the Schell Creek Range, which is based on the average of 11 three-point problems (Table S2; see text footnote 1). This is consistent with the minimum dips required for B1 (27°W), B2 (21°W), and B3 (20°W) to not intersect the modern surface to the west of their traces, and defines average cutoff angles of 8° for all four detachments.

4 - The 35°W average apparent dip of Z-MIP rocks in the Schell Creek Range (n=71), when combined with the 34°W average apparent dip of Pg on the western flank of the Schell Creek Range, defines 1° of angularity across the Paleogene unconformity here (cutting down-section toward the east).

5 - The syncline with Pg in its hinge zone shown beneath Duck Creek Valley is supported by average apparent dip angles of attitude measurements of Pg from Young (1960) that are projected from 0-5 km to the north of the section line (n=7 from eastern limb) and 7-8 km north of the section line (n=8 from eastern limb, n=4 from axial zone of syncline, and n=8 from western limb of syncline).

6 - An average apparent dip of 16°W for NgQ was calculated from 12 bedding measurements: 7 from Young (1960) are within 0-2 km of the section line, and 5 from Anderson (1983) are projected from 5-6 km N of the section line. This, combined with the 16°W average apparent dip of NgQ valley fill in the Spring Valley half-graben, was utilized to retrodeform 15° of westward tilting for the entire width of the restored cross section.

7 - Bedding measurements from unit Cl define a 36°W average apparent dip for the western limb of the culmination in the western Duck Creek Range, and balancing constraints require a 28°E dip for the eastern limb of the culmination under the eastern Duck Creek Range and the western part of Duck Creek Valley.

Figure 5. (A) Cross-section B-B′, showing the modern geometry. Schell Creek Range detachment system (SCRDS) faults B1–B5 are labeled, and bold italic numbers are referenced to footnotes. The subsurface geometry for Spring Valley and the western part of the Northern Snake Range is from the interpreted seismic cross section of Gans et al. (1985, their fig. 2). Translucent areas above the modern surface represent eroded rock. (B) Cross-section B-B′ after retrodeformation of displacement on post–Schell Creek Range detachment system high-angle normal faults and 15° of post–Schell Creek Range detachment system westward tilting (see footnote 2). Stratigraphic cutoff angles are labeled for Schell Creek Range detachment system faults. NSRD—Northern Snake Range décollement.

(Figs. 1 and 6; Fig. S1C). The subsurface geometry of Spring Valley to the east is constrained by the interpreted seismic cross section of Gans et al. (1985) (location shown on Fig. 1).

Post–Schell Creek Range detachment system normal faults on cross-section B-B′ dip ~40–60°E, with the exception of the Kalamazoo fault, which dips 83°W (Fig. 5; Table 1). The Schell Creek fault accommodated 10.5 km of top-down-to-the-E displacement, resulting in the subsidence and infilling of the Spring Valley half graben (Gans et al., 1985). The valley-fill sediments in Spring Valley thicken westward, and the unconformity at their base has an average dip of 14.5°W (Gans et al., 1985). The Duck Creek fault accommodated 1.2 km of top-down-to-the-E displacement (Table 1), which resulted in the subsidence and infilling of the Duck Creek Valley half graben (Anderson, 1983). The valley-fill unit (the North Creek Formation of Young, 1960) thickens westward and has an average dip of 16°W (Fig. 5). Retrodeformation of displacement on all post–Schell Creek Range detachment system normal faults on cross-section B-B′, combined with restoration of 15° of westward tilting (the average of the Duck Creek Valley and Spring Valley half grabens), defined 9.9 km of extension (61%).

Four Schell Creek Range detachment system faults (B1, B2, B3, B5) were mapped along cross-section B-B′ in the western part of the Schell Creek Range (Figs. 1 and 5; Figs. S1C, S3B, and S4A), and they are shown at a dip angle of 27°W, which is the average of 11 three-point problems (Table 2; Table S3) and defines an average stratigraphic cutoff angle of 8° for these faults. The lowest detachment fault (B1) omits 0.8 km of unit Cu. The second lowest detachment fault (B2) omits 0.05 km of unit Cu, and the third lowest (B3) places unit OS on the upper part of unit Cu and omits 0.6 km of stratigraphy. The highest detachment fault (B5) places unit MIP over unit OS, omitting 2.3 km of stratigraphy. Crosscutting relationships indicate that the detachments become younger moving structurally upward; for example, B3 cuts downward to the east across B2 ~1.5 km south of the B-B′ section line (Fig. 1; Fig. S1C).

Paleogene volcanic rocks overlie unit MIP on the western flank of the Schell Creek Range, and average apparent dips above and below the basal Paleogene unconformity define 1° of angularity (Fig. 5). To the west, the Schell Creek Range detachment system is concealed under Duck Creek Valley. Apparent dips projected from 0 to 8 km to the north of the section line show that the Paleogene section is deformed into an open syncline in the subsurface (~35°W-dipping eastern limb, ~15°E-dipping western limb). Several field relationships in the eastern half of the Duck Creek Range support this interpretation, including the gentle eastward dip (typically ~10°–20°) of Devonian–Pennsylvanian rocks, detachment faults B4 and B5, and the Paleogene unconformity (which overlies the same Pennsylvanian unit as in the western Schell Creek Range; Table 1; Fig. 6). Therefore, we show a syncline with unit Pg in its hinge zone in the subsurface of Duck Creek Valley on cross-section B-B′, which also folds the Schell Creek Range detachment system, similar to our interpretation for cross-section A-A′ (Fig. 5).

In the Duck Creek Range, a stacked series of Schell Creek Range detachment system faults carry sheets of Cambrian–Pennsylvanian rocks that are as thin as ~30–70 m, exhibit stratigraphic cutoff angles typically between 5° and 10°, and are folded into an open, antiformal structural culmination (Figs. 5 and 6). Five detachment faults (B1–B5) are present. Based on subsurface projection of cutoff angles, faults B1, B2, B3, and B5 were correlated with their traces in the Schell Creek Range. Observations in the Duck Creek Range that support folding of the Schell Creek Range detachment system include: (1) the ~10°–20°E dip of Devonian–Pennsylvanian rocks, the Paleogene unconformity, and detachment faults B4 and B5 in the eastern half of the range; (2) an anticline axis mapped within unit Cl that separates the 36°W-dipping western limb of the culmination from the 7°E-dipping culmination crest zone; (3) multiple traces of B1 that constrain a 5°E dip at the range crest and a 17°W dip on the western flank of the range; (4) a 26°W dip for B3 on the western flank of the range; and (5) a 21°W dip for the Paleogene unconformity at the western edge of the cross section. The Schell Creek Range detachment system accomplished extreme structural attenuation in the Duck Creek Range, with 5.3 km of cumulative stratigraphic omission at the culmination axis, where Pennsylvanian rocks lie only 0.15 km structurally above Lower Cambrian rocks. Crosscutting relationships demonstrate that faults of the Schell Creek Range detachment system become progressively younger moving structurally upward; for example, B3 cuts B2, and B4 cuts B3 (Fig. 6). Also, Young (1960) described NNE-trending drag folds that define an ESE-directed sense of motion for fault B5 at a location ~1 km north of the B-B′ section line, and for a fault that is likely equivalent to B3 at a location ~4 km north of the B-B′ section line.

Retrodeformation of the Schell Creek Range detachment system on cross-section B-B′ (Fig. 4B) yielded 14.5 km of top-down-to-the-E displacement on B1, 0.6 km on B2, 5.1 km on B3, 6.5 km on B4, and 9.3 km on B5, defining a cumulative displacement magnitude of 36.0 km. The cumulative east-west extension accommodated by the Schell Creek Range detachment system on B-B′ is 35.2 km (Fig. 4B). Another important observation is that the lowest detachment fault (B1) cuts down to the top of unit Cl in the Duck Creek Range, which requires that the Schell Creek Range detachment system had rooted to an approximate stratigraphic flat by the longitude of the culmination axis. This flat can be traced for ~13 km between the culmination axis and the eastern edge of cross-section B-B′ (Fig. 4B).

Cross-Section C-C′

Cross-section C-C′ (Fig. 7) is supported by the mapping of Drewes (1967) (Fig. S1D) and is supplemented by the mapping of Walker et al. (1992) on its western side. The following discussion is also supported by a detailed geologic map (Fig. 8) of a portion of the Duck Creek Range that lies ~1–8 km north of cross-section C-C′, which was compiled from Drewes (1967), our mapping, and Walker et al. (1992), and two accompanying cross sections (D-D′ and E-E′; Fig. 9).

Post–Schell Creek Range detachment system normal faults on cross-section C-C′ exhibit displacements on the order of 0.15–0.75 km (Table 1). Displacement on the Schell Creek fault is not constrained on cross-section C-C′, and the magnitude of post–detachment system westward tilting is also not constrained but

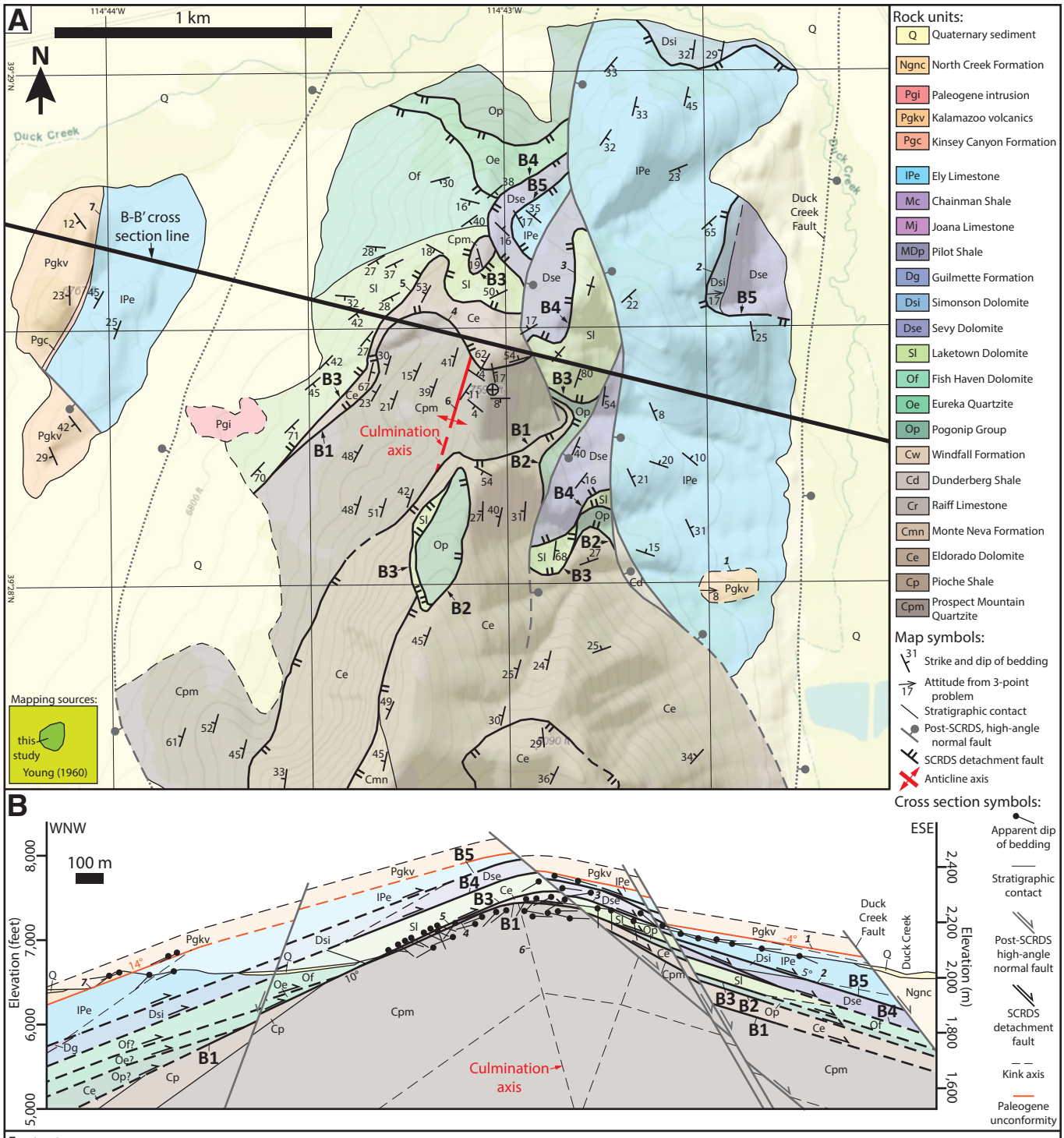

Footnotes:

1 - A three-point problem from the Pgkv over IPe unconformity 0.5 km S of the section line yields an 8°E dip. When combined with the 12°E average apparent dip of IPe, this defines an angularity of -4° (cuts upsection toward the east).
2 - For detachment B5, a three-point problem 0.4 km north of the section line defines a dip of 17°E. When combined with the 12°E average dip of IPe, this defines a hanging wall cutoff angle of 5°.
3 - Near the range crest, detachment B4 must dip 21°E or less to not intersect the modern surface to the east of its trace.
4 - The section line crosses three separate traces of detachment B1; the eastern and middle traces constrain a dip of 5°E, and the middle and western traces constrain a dip of 17°W.
5 - Detachment B3 must dip at least 26°W to not intersect the modern surface to the west of its trace, and its map pattern to the south of the section line suggests that this must be close to the true dip angle. When combined with the average apparent dip of Cpm, this defines a footwall cutoff angle of 10°.
6 - Bedding measurements of Cpm define a 36°W average apparent dip for the western limb of the culmination (n=8) and a 7°E dip for the axial zone at the range crest (n=5). Balancing constraints on Figure 5 constrain a 28°E dip for the eastern limb of the culmination under the eastern Duck Creek Range and the western part of Duck Creek Valley.
7 - Bedding measurements from IPe (n=2) define a 35°W average apparent dip, and measurements from Pgkv (n=4) define a 21°W average apparent dip, defining 14° of angularity (cutting downsection to the east) for the basal Pgkv unconformity on the western edge of the cross section.

Figure 6. (A) Detailed geologic map of the Duck Creek Range at the latitude of cross-section B-B′ (location shown on Fig. 1C), compiled from Young (1960) and our mapping. Schell Creek Range detachment faults B1–B5 are labeled, and bold italic numbers are referenced to footnotes. (B) Detailed cross section of the portion of B-B′ that passes through the Duck Creek Range, illustrating folding of the Schell Creek Range detachment system (SCRDS) across the anticlinal culmination.

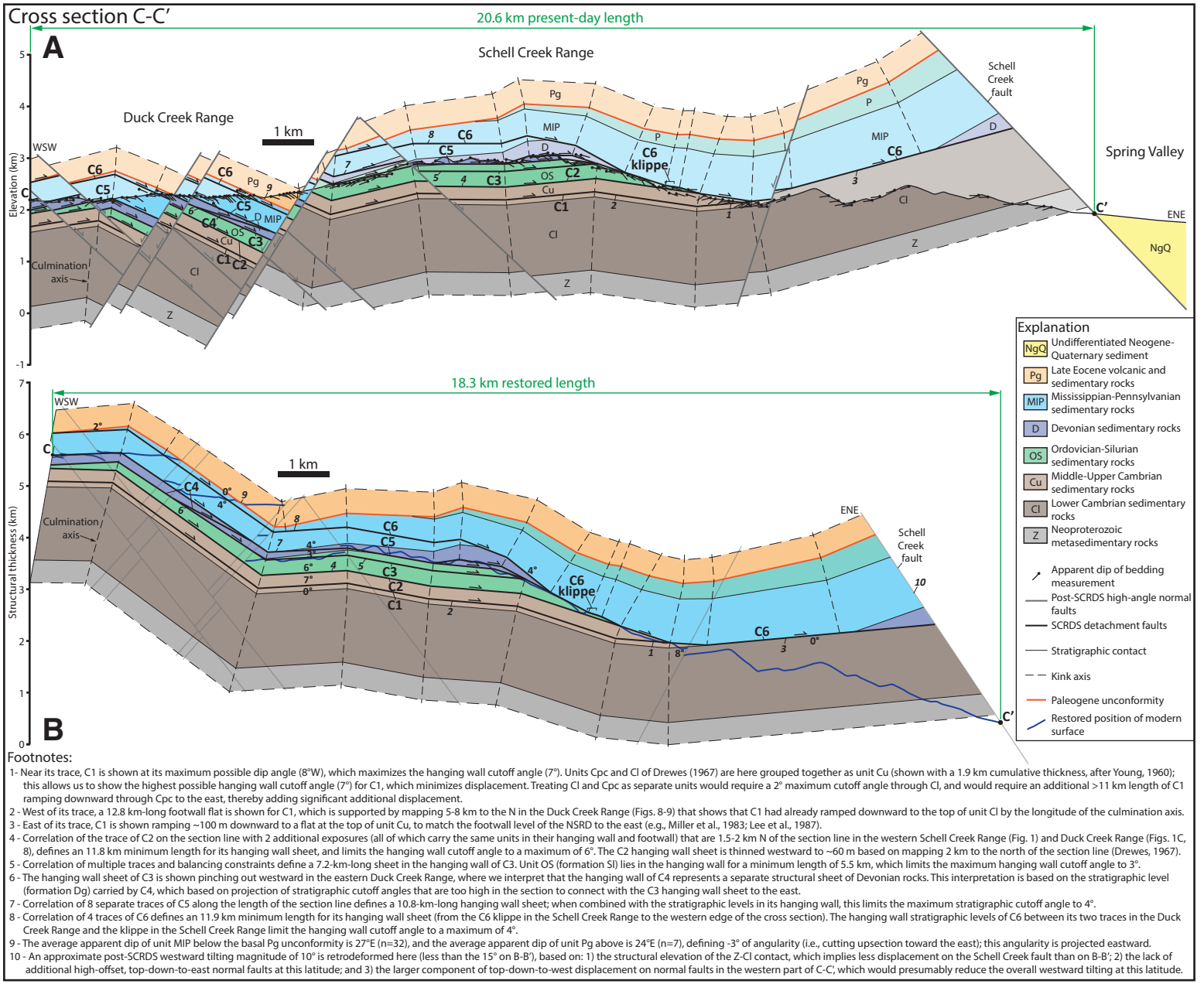

Figure 7. (A) Cross-section C-C′, showing the modern geometry. Schell Creek Range detachment system (SCRDS) faults C1–C6 are labeled, and bold italic numbers are referenced to footnotes. Translucent areas above the modern surface represent eroded rock. (B) Cross-section C-C′ after retrodeformation of displacement on post–Schell Creek Range detachment system normal faults and 10° of post–Schell Creek Range detachment system westward tilting (see footnote 10). Stratigraphic cutoff angles are labeled for Schell Creek Range detachment faults. NSRD—Northern Snake Range décollement.

Footnotes:

1- Near its trace, C1 is shown at its maximum possible dip angle (8°W), which maximizes the hanging wall cutoff angle (7°). Units Cpc and Cl of Drewes (1967) are here grouped together as unit Cu (shown with a 1.9 km cumulative thickness, after Young, 1960); this allows us to show the highest possible hanging wall cutoff angle (7°) for C1, which minimizes displacement. Treating Cl and Cpc as separate units would require a 2° maximum cutoff angle through Cl, and would require an additional >11 km length of C1 ramping downward through Cpc to the east, thereby adding significant additional displacement.

2 - West of its trace, a 12.8 km-long footwall flat is shown for C1, which is supported by mapping 5-8 km to the N in the Duck Creek Range (Figs. 8-9) that shows that C1 had already ramped downward to the top of unit Cl by the longitude of the culmination axis.

3 - East of its trace, C1 is shown ramping ~100 m downward to a flat at the top of unit Cu, to match the footwall level of the NSRD to the east (e.g., Miller et al., 1983; Lee et al., 1987).

4 - Correlation of the trace of C2 on the section line with 2 additional exposures (all of which carry the same units in their hanging wall and footwall) that are 1.5-2 km N of the section line in the western Schell Creek Range (Fig. 1) and Duck Creek Range (Figs. 1C, 8), defines an 11.8 km minimum length for its hanging wall sheet, and limits the hanging wall cutoff angle to a maximum of 6°. The C2 hanging wall sheet is thinned westward to ~60 m based on mapping 2 km to the north of the section line (Drewes, 1967).

5 - Correlation of multiple traces and balancing constraints define a 7.2-km-long sheet in the hanging wall of C3. Unit OS (formation Sl) lies in the hanging wall for a minimum length of 5.5 km, which limits the maximum hanging wall cutoff angle to 3°.

6 - The hanging wall sheet of C3 is shown pinching out westward in the eastern Duck Creek Range, where we interpret that the hanging wall of C4 represents a separate structural sheet of Devonian rocks. This interpretation is based on the stratigraphic level (formation Dg) carried by C4, which based on projection of stratigraphic cutoff angles that are too high in the section to connect with the C3 hanging wall sheet to the east.

7 - Correlation of 8 separate traces of C5 along the length of the section line defines a 10.8-km-long hanging wall sheet; when combined with the stratigraphic levels in its hanging wall, this limits the maximum stratigraphic cutoff angle to 4°.

8 - Correlation of 4 traces of C6 defines an 11.9 km minimum length for its hanging wall sheet (from the C6 klippe in the Schell Creek Range to the western edge of the cross section). The hanging wall stratigraphic levels of C6 between its two traces in the Duck Creek Range and the klippe in the Schell Creek Range limit the hanging wall cutoff angle to a maximum of 4°.

9 - The average apparent dip of unit MIP below the basal Pg unconformity is 27°E (n=32), and the average apparent dip of unit Pg above is 24°E (n=7), defining -3° of angularity (i.e., cutting upsection toward the east); this angularity is projected eastward.

10 - An approximate post-SCRDS westward tilting magnitude of 10° is retrodeformed here (less than the 15° on B-B′), based on: 1) the structural elevation of the Z-Cl contact, which implies less displacement on the Schell Creek fault than on B-B′; 2) the lack of additional high-offset, top-down-to-east normal faults at this latitude; and 3) the larger component of top-down-to-west displacement on normal faults in the western part of C-C′, which would presumably reduce the overall westward tilting at this latitude.

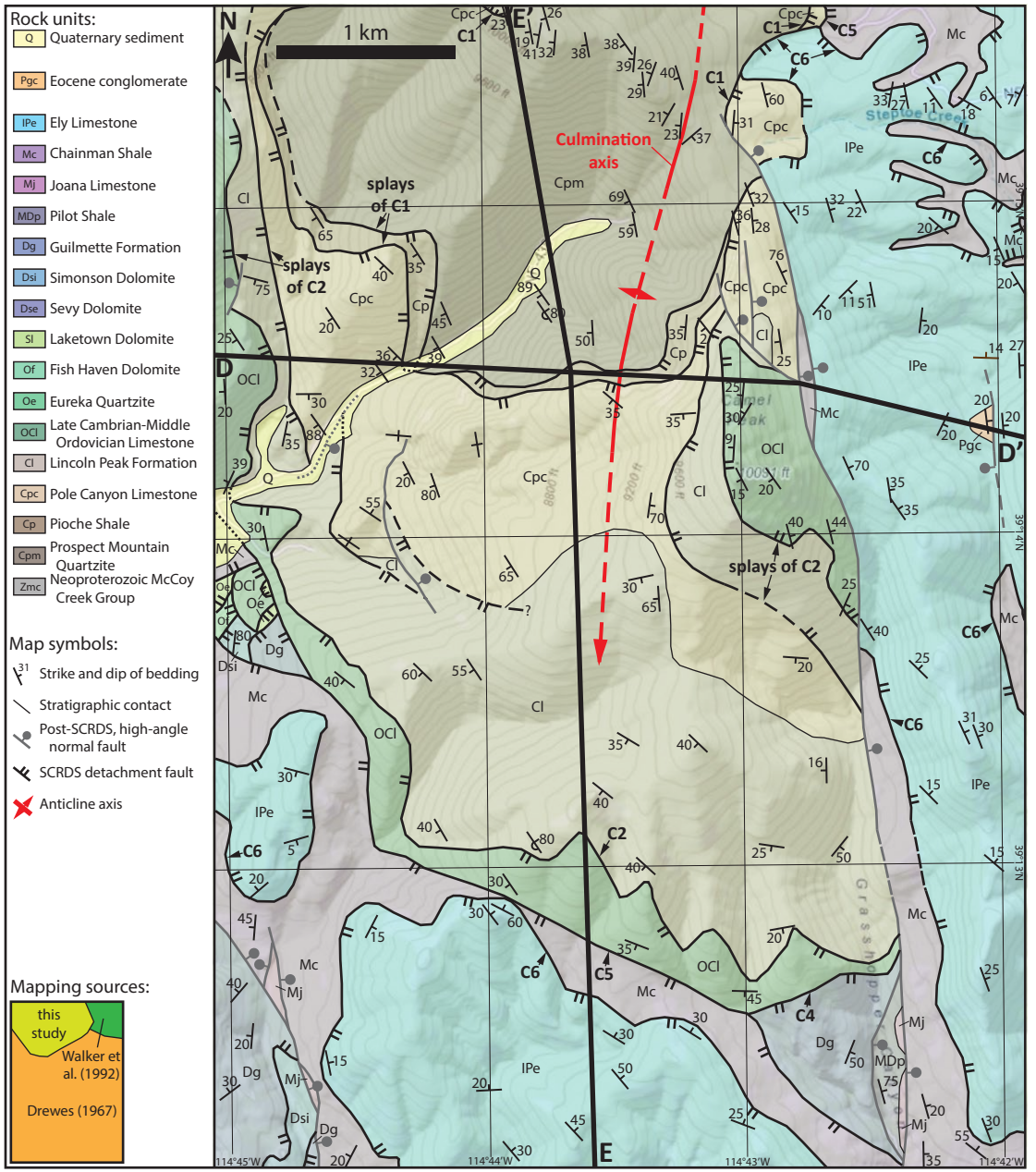

Figure 8. Detailed geologic map of a portion of the Duck Creek Range between ~1 and 8 km to the north of the C-C′ section line (location shown on Fig. 1C), compiled from Drewes (1967), our mapping, and Walker et al. (1992). Schell Creek Range detachment system (SCRDS) faults C1–C6 are labeled (C1 and C2 are locally mapped as two separate splays).

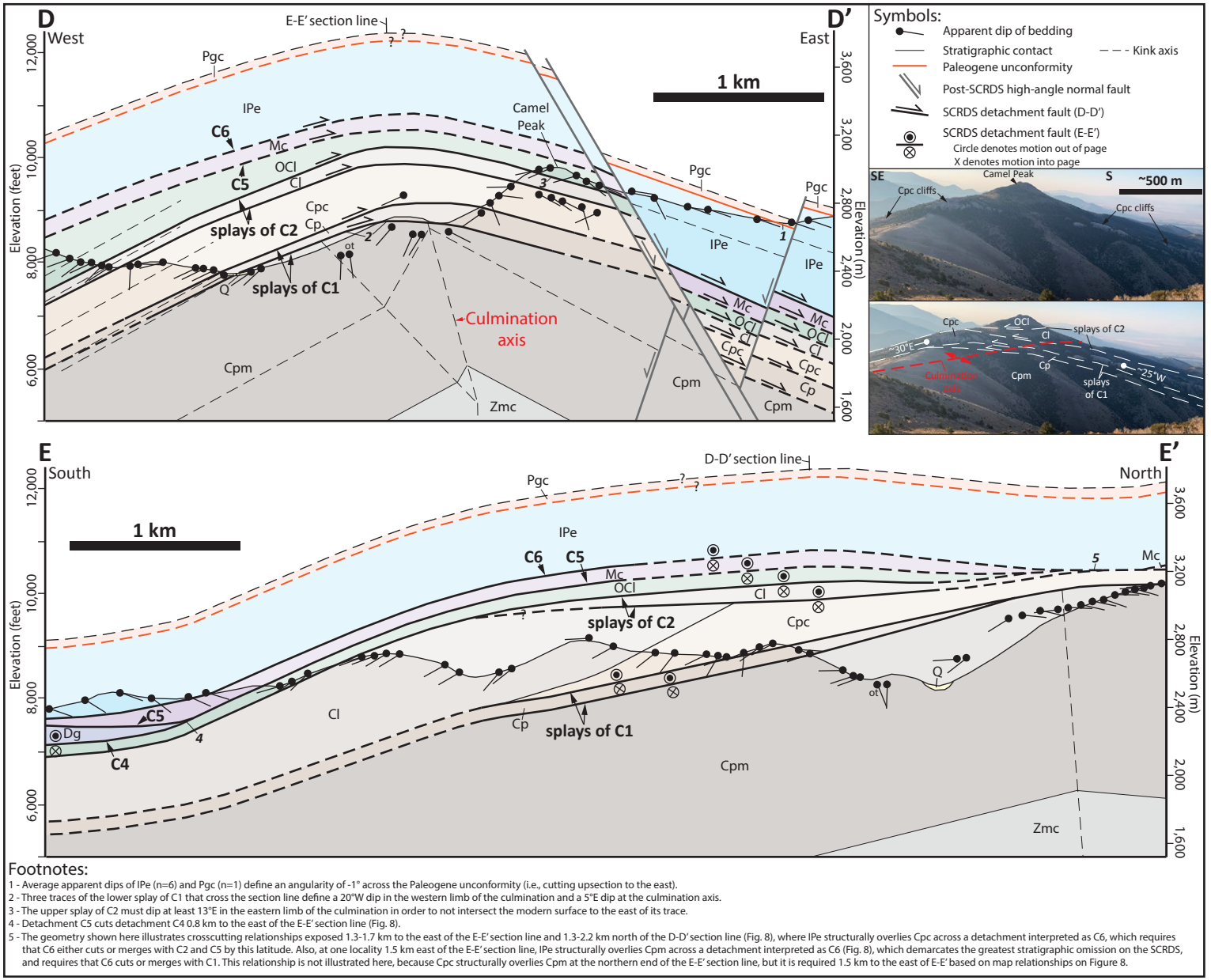

Figure 9. Cross-sections D-D′ and E-E′ through the southern portion of the Duck Creek Range (lines of section shown on Figs. 1 and 8). Cross-section D-D′ illustrates the folding of the Schell Creek Range detachment system (SCRDS) across the antiformal culmination, and cross-section E-E′ illustrates along-strike patterns of extreme structural attenuation approximately parallel to the culmination axis. Detachments C1–C6 are labeled, and bold italic numbers are referenced to footnotes. See Figure 8 for a guide to rock unit abbreviations. Field photographs on the right show original (top) and annotated (bottom) versions that illustrate folding of the splays of faults C1 and C2 across the culmination axis.

is approximated at 10° (see Fig. 7, footnote 10). Retrodeformation of post–Schell Creek Range detachment system normal faults yielded 2.3 km of minimum extension (13%; Fig. 7).

Six detachment faults are present on cross-section C-C′ (C1–C6), and they carry sheets that are up to 13 km long and typically between 0.2 and 0.4 km thick (Fig. 7). A combination of three-point problems and geometric constraints between multiple traces that intersect the section line (Fig. 7, footnotes; Table 2; Table S3) showed that detachment faults generally dip ~5°–15°E in the eastern Schell Creek Range, are subhorizontal near the Schell Creek Range crest, and are folded into an open antiformal culmination in the Duck Creek Range. Detachment faults C1–C6 were drafted at their maximum possible cutoff angles (typically between 3° and 7°; Figs. 4 and 7, footnotes). The Paleogene unconformity is exposed in one locality each on cross-section C-C′ and in Figures 8 and 9, where it overlies Pennsylvanian rocks and exhibits minimal (≤3°) angularity.

The structurally lowest detachment fault (C1) is exposed in the eastern Schell Creek Range (Fig. 1C; Fig. S1D), where its footwall level lies 100 m stratigraphically above the top of unit Cl, and it is correlated with the lowest detachment in the Duck Creek Range culmination zone (Figs. 8 and 9; Figs. S3A and S4B), which consists of two splays that deform the top portion of unit Cl (formations Cpm and Cp). Similar to cross-section B-B′, this indicates that the basal detachment fault had ramped downward approximately to the Cl-Cu contact by the longitude of the Duck Creek Range, thus requiring a 12.8-km-long footwall flat between the western edge of cross-section C-C′ and the trace of C1 in the Schell Creek Range (Figs. 4 and 7; Fig. S3A). C1 omits up to 1.55 km of stratigraphy and accommodated 12.8 km of displacement.

Detachment fault C2 omits up to 1.1 km of units Cu and OS and accommodated 11.9 km of displacement. Detachment fault C3 omits 1.1 km of unit OS and has 10.9 km of displacement. Detachment fault C4 was only observed in the Duck Creek Range, where it omits 0.3 km of unit D and has 4.3 km of displacement. Correlation of detachment fault C5 between traces in the Schell Creek Range, where it places unit D over unit OS, and traces in the Duck Creek Range, where it places unit MIP over unit D, shows that this fault omits up to 0.65 km of stratigraphy and accommodated 4.5 km of displacement. As documented on cross-sections A-A′ and B-B′, Schell Creek Range detachment faults on cross-section C-C′ become successively younger with increasing structural height; for example, C3 cuts C2, C5 cuts C4, and C6 cuts C5 and C1 (Table 2; Fig. 8).

Detachment C6 was correlated between multiple traces in the Duck Creek Range that deform unit MIP (placing formation IPe over formation Mc; Fig. 8) and a klippe of unit MIP in the Schell Creek Range that overlies unit OS in the hanging wall of C2 (the "C6 klippe" on Figs. 1, 4, and 7). The preservation of this klippe requires that C6 must cut structurally downward to the east across detachment faults C5 and C3 above the modern surface (Fig. 7). Detachment fault C6 was mapped by Drewes (1967) as cutting the basal conglomerate of unit Pg between 2 and 8 km south of cross-section C-C′ (Fig. 1). C6 omits 0.05 km of unit MIP in the Duck Creek Range, omits 3.05 km of stratigraphy beneath the klippe in the Schell Creek Range, and accommodated 7.5 km of displacement.

On the western end of cross-section C-C′, average apparent dips of units D and MIP define an antiformal culmination with a 27°E-dipping eastern limb and a 16°W-dipping western limb. Well-exposed field relations 4–8 km to the north of cross-section C-C′ illustrate folding of multiple detachment faults across the culmination (Figs. 8 and 9; Fig. S4B). Here, detachment faults C1 and C2 (each consisting of two separate splays) are deformed into an open antiform, with the rocks in their hanging wall and footwall generally dipping ~25°W in the western limb and ~20°–30°E in the eastern limb. Cross-section D-D′ crosses multiple traces of the lower splay of C1, which defines an eastward transition from a 20°W dip to a 5°E dip as the culmination axis is crossed, and the upper splay of C2 must dip at least 15°E in the eastern limb of the culmination (Fig. 9, footnotes). Field relationships illustrate extreme stratigraphic attenuation over the culmination axis, including 5.0 km of cumulative omission on cross-section D-D′, where Pennsylvanian rocks above C6 are separated from Lower Cambrian rocks below C1 by five detachment-bounded sheets with a cumulative structural thickness of 0.6 km (Fig. 9). We documented a similar omission magnitude ~1.7 km to the north of cross-section D-D′ (Fig. 8), where Pennsylvanian rocks overlie Lower Cambrian rocks across detachment C6, which defines 5.2 km of omission.

The cumulative displacement on the Schell Creek Range detachment system on cross-section C-C′ is 51.9 km, and the minimum cumulative east-west extension accommodated by the detachment system across cross-section C-C′ is 51.5 km (Fig. 4C). However, as discussed in the following section, we interpret that cross-section C-C′ was likely drafted oblique to the transport direction of the Schell Creek Range detachment system, and therefore this displacement estimate may not be representative.

INTERPRETATION OF THE GEOMETRY, KINEMATICS, AND MAGNITUDE OF EXTENSION ON THE SCHELL CREEK RANGE DETACHMENT SYSTEM

An interpretive model for the Schell Creek Range detachment system must explain the following first-order observations:

(1) The Schell Creek Range detachment system is an integrated system of top-down-to-the-E, brittle faults with ~5°–10° stratigraphic cutoff angles, with the geometry of an upward-younging imbricate stack that carries sheets on the order of ~0.1–0.5 km thick and up to ~8–13 km long.

(2) The western portion of the Schell Creek Range detachment system is folded across an antiformal culmination with an interlimb angle of 120°–135° and an eastern limb with a structural height of 1.5–2.0 km and a map length of 2.8–3.1 km. In the crest zone of the culmination, structurally lower sheets are often incised or cut out by structurally higher detachments, resulting in greater stratigraphic omission (up to 5.2–5.3 km) compared to the thicker imbricate stack to the east in the Schell Creek Range (up to 3.7–4.6 km). The increase in omission with proximity to the culmination axis supports a scenario of progressive synextensional growth of the culmination (Long and Walker, 2015).

(3) The basal Paleogene unconformity in the Schell Creek and Duck Creek Ranges exhibits minimal angularity (typically 0°–3°) and low structural relief (0.7 km total) with respect to underlying Paleozoic rocks (Young, 1960; Drewes, 1967), which is also observed in many of the surrounding ranges (e.g., Kellogg, 1963; Fritz, 1968; Moores et al., 1968; Armstrong, 1972; Hose and Blake, 1976; Gans and Miller, 1983; Rodgers, 1987; Long, 2012, 2015). Therefore, Paleozoic rocks had shallow dip angles prior to extension on the Schell Creek Range detachment system, which indicates that the ~5°–10° stratigraphic cutoff angles of detachment faults approximate the angles at which they initiated.

(4) Schell Creek Range detachment faults cut rocks as shallow as the base of the Paleogene section, which were likely within ~1 km of the paleosurface (e.g., Armstrong, 1972; Gans and Miller, 1983). This indicates that the exposed levels of the Schell Creek Range detachment system were active at a paleodepth range of ~1–7 km, which is consistent with the breccia zones observed along detachment faults (Fig. S2).

We interpret that the Schell Creek Range detachment system records the progressive evolution of the breakaway zone of a low-angle, top-down-to-the-E detachment fault system. Key aspects of the geometry and kinematics of the Schell Creek Range detachment system are well explained by the process of excision, whereby a detachment fault system evolves by cutting progressively upward into its hanging wall (Lister and Davis, 1989). In the excision model, an actively slipping detachment becomes progressively domed due to isostatic rebound induced by structural thinning (Fig. 4D). Eventually, the portion of the detachment updip of the axis of doming becomes back-tilted to a point where it becomes mechanically favorable to form a new, structurally higher detachment, thereby accreting a thin sheet of rock to the footwall. The number of preserved sheets in the Schell Creek Range detachment system indicates that this process took place at least three to five times. With continued displacement and isostatic rebound, an anticlinal culmination that folds the detachment system is progressively constructed. Continued uplift results in incision of structurally lower sheets above the culmination axis, which increases structural attenuation, and thus acts as a positive feedback process that promotes a stationary, long-duration site of isostatic uplift (the "fixed hinge" of Long and Walker, 2015). Long et al. (2018) demonstrated that the axis of uplift is predicted to be located at the approximate point where the detachment fault roots to a footwall flat. The geometries of cross-sections B-B′ and C-C′ support this prediction for the Schell Creek Range detachment system (A-A′ does not exhibit this geometry, but this is likely the consequence of our assumption that there are no detachments below A4 in the Duck Creek Range). The final geometry is a stacked series of long, thin, detachment-bounded sheets, which were progressively emplaced from bottom to top.

Cumulative displacement on the Schell Creek Range detachment system appears to increase southward, from 16.8 km on cross-section A-A′, to 36.0 km on B-B′, to 51.9 km on C-C′. However, the displacement magnitude on cross-section A-A′ is likely an underestimate, as we used the maximum possible cutoff angles for detachments A1–A3, and we assumed that there are no detachments beneath A4 in the Duck Creek Range. Also, due to differences in the average strike direction of detachment faults, the C-C′ section line is oriented 35° counterclockwise to cross-sections A-A′ and B-B′ (Fig. 1C). We consider the 105° strike-normal azimuth of cross-sections A-A′ and B-B′ to likely be the most representative for the average transport direction of Schell Creek Range detachment system, based on the top-to-the-ESE motion direction for the faults B3 and B5 indicated by drag folding (Young, 1960), and the similarity to the 110°–125° transport direction of the Northern Snake Range décollement to the east (e.g., Miller et al., 1983; Lee et al., 1987). Therefore, we speculate that the 070° azimuth of cross-section C-C′ is oriented oblique to the Schell Creek Range detachment system transport direction. Given that the total number of detachments, as well as the stratigraphic levels that they occupy, can change over relatively short distances along strike (e.g., Young, 1960; Drewes, 1967; also see Figs. 1, 6, 8, and 9), we speculate that the 51.9 km cumulative displacement for cross-section C-C′ may not be a representative estimate for this fault system. Therefore, from this point forward, we consider the 36.0 km cumulative displacement estimate from cross-section B-B′ to be the most representative for the Schell Creek Range detachment system.

CONSTRAINTS ON THE TIMING OF EXTENSION ON THE SCHELL CREEK RANGE DETACHMENT SYSTEM

The minimal angularity and structural relief across the basal Paleogene unconformity (Young, 1960; Gans and Miller, 1983; this study), combined with a lack of map evidence for any detachment faults being truncated by the unconformity (Young, 1960; Drewes, 1967), indicate that large-scale displacement on the Schell Creek Range detachment system must have postdated deposition of the late Eocene Kinsey Canyon Formation (the basal Paleogene clastic unit).

Along and proximal to cross-sections A-A′ and C-C′, the structurally highest detachment faults (faults A4 and C6) cut the basal part of the Paleogene section (Young, 1960; Drewes, 1967). On cross-section A-A′, detachment fault A4 cuts as high in the section as the basal unit of the Kalamazoo volcanic rocks (Young, 1960), indicating that displacement on this fault initiated after ca. 36.1–35.2 Ma ($^{40}Ar/^{39}Ar$ sanidine; Druschke et al., 2009). Between 2 and 8 km to the south of section C-C′, detachment C6 cuts the Kinsey Canyon Formation (Drewes, 1967), indicating that displacement on this fault initiated after ca. 36.5–35.2 Ma ($^{40}Ar/^{39}Ar$ sanidine and U-Pb zircon; Druschke et al., 2009, 2011).

Intraformational angular unconformities between Paleogene rock units have been used to support interpretations for a synvolcanic initiation of extension-related tilting in the Schell Creek Range. Near cross-section C-C′, Druschke et al. (2009) described up to 20° of local differential eastward and westward tilting between the Kinsey Canyon Formation and the overlying Kalamazoo volcanic rocks, which brackets tilting and erosional beveling of the Kinsey Canyon Formation between ca. 35.5 and ca. 35.2 Ma ($^{40}Ar/^{39}Ar$ sanidine). Near cross-section A-A′, Gans and Miller (1983) and Gans et al. (1989)

described local differential tilting between ca. 36.0 and 35.8 Ma (K/Ar biotite) tuffs and lavas of the Kalamazoo volcanic rocks.

The primary field relationship that brackets the cessation of displacement on the Schell Creek Range detachment system is the onset of deposition of the North Creek Formation in Duck Creek Valley, which was deposited in a gently west-tilted half graben generated by displacement on the Duck Creek fault (Young, 1960; Anderson, 1983; Gans and Miller, 1983). The North Creek Formation overlies the Kalamazoo volcanic rocks across an angular unconformity and postdates the folding of these volcanic rocks into an open syncline that we attribute to construction of the eastern limb of the culmination that folds the Schell Creek Range detachment system (Figs. 1C and 5). The Duck Creek fault cuts multiple Schell Creek Range detachment faults (Young, 1960; Figs. 1C, 3, and 5), and its initiation is interpreted to demarcate a transition to an episode of lower-magnitude extension along high-angle, latest Paleogene to Neogene normal faults (Anderson, 1983; Gans et al., 1985, 1989). Therefore, we interpret that deposition of the 28.7–26.1 Ma (zircon fission-track dating; Anderson, 1983) vitric tuff near the base of the North Creek Formation brackets the youngest possible age for the cessation of displacement on the Schell Creek Range detachment system.

In summary, field relationships and geochronology of Paleogene rocks bracket large-scale displacement along the Schell Creek Range detachment system between ca. 36.5 and 26.1 Ma (late Eocene to late Oligocene).

DISCUSSION

The Schell Creek Range detachment system is characterized by as many as six low-angle, top-down-to-the-ESE, brittle detachment faults that cut across late Eocene volcanic and sedimentary rocks and the thick, underlying Paleozoic sedimentary section of eastern Nevada. On the basis of their spatial proximity, their compatible displacement sense, their overlapping deformation timing, as well as the similar Lower Cambrian stratigraphic level to which they root, we interpret that the Schell Creek Range detachment system represents the western breakaway zone for the Northern Snake Range décollement to the east (Fig. 1B). In the following sections, we discuss our arguments for genetically relating high-magnitude, top-down-to-the-ESE extension on the Schell Creek Range detachment system to the Northern Snake Range décollement. Our discussion is supported by cross-section F-F′ across the Northern Snake Range (Fig. 10A; line of section shown on Fig. 1B), which utilizes the 1:24,000 scale geologic map compilation of Johnston (2000). The F-F′ section line is drawn at an azimuth of 117.5°, which is the average trend of mineral stretching lineations in the Northern Snake Range décollement footwall and is interpreted as the best estimate for the extension direction (Miller et al., 1983; Lee et al., 1987).

The present-day structural framework of the Northern Snake Range has been established in detail (e.g., Miller et al., 1983; Gans et al., 1985; Lee et al., 1987), yet there remains a long-standing debate over the pre-extensional depth of Neoproterozoic–Lower Cambrian metasedimentary rocks in the Northern Snake Range décollement footwall, and the corresponding implications for the original geometry, depth, and displacement magnitude of this structure. Earlier studies proposed that the Northern Snake Range décollement originated as an ~7-km-deep, subhorizontal zone of decoupling between brittlely deformed rocks above, which restore to ~0–7 km pre-extensional stratigraphic depths, and ductilely stretched metasedimentary rocks below, which restore to pre-extensional stratigraphic depths of ~7–12 km (Gans and Miller, 1983; Miller et al., 1983; Gans et al., 1985; Lee et al., 1987). In contrast, other studies have presented structural arguments (Bartley and Wernicke, 1984; Wrobel et al., 2021) and thermobarometry data (Lewis et al., 1999; Cooper et al., 2010) that suggest that rocks in the footwall of the Northern Snake Range décollement were buried as deep as ~20–30 km prior to extension, potentially up to ~3 times greater than their original stratigraphic depths. Attainment of these depths has been attributed to burial during Cretaceous structural thickening (Bartley and Wernicke, 1984; Lewis et al., 1999; Wrobel et al., 2021).

The disagreement over the pre-extensional geometry of the Northern Snake Range metamorphic core complex remains unresolved, as several field relationships (summarized in Miller et al., 1999a) provide strong arguments that rocks above and below the Northern Snake Range décollement were stratigraphically contiguous prior to extension. In addition, a recent cross-section restoration across eastern Nevada and western Utah did not find evidence for large-scale contractional structures that could have accommodated deep structural burial in the region surrounding the Northern Snake Range (Blackford et al., 2022). Other factors contributing to this debate include recent studies in the Ruby–East Humboldt metamorphic core complex in northeastern Nevada, which argue that pre-extensional structural burial depths of footwall rocks were much shallower than thermobarometric estimates (Henry et al., 2011; Zuza et al., 2020), allowing for the possibility that these rocks experienced tectonic overpressure (Zuza et al., 2022). Also, Hoiland (2019), based on analysis of temperature and pressure data, tentatively interpreted that rocks in the Northern Snake Range experienced tectonic overpressure that may have generated a departure from lithostatic pressures by up to a factor of two.

As our study is focused on describing the geometry and kinematics of extension in the Schell Creek and Duck Creek Ranges, the resolution of the long-standing debate over the pre-extensional geometry of the Northern Snake Range metamorphic core complex is beyond the scope of this paper. Given this, we present a restored version of a cross section across the Northern Snake Range (Fig. 11B) that illustrates a simple pre-extensional geometry that: (1) follows the interpretations of Gans and Miller (1983), Miller et al. (1983), and Gans et al. (1985), wherein the Northern Snake Range décollement restores to an ~7-km-deep, subhorizontal geometry; (2) assumes that rocks in the footwall of the Northern Snake Range décollement restore to an original stratigraphic depth range of ~7–12 km; and (3) utilizes the finite strain data of Lee et al. (1987) to reconstruct the pre-extensional dimensions of rocks in the Northern Snake Range décollement footwall. Nevertheless, we acknowledge

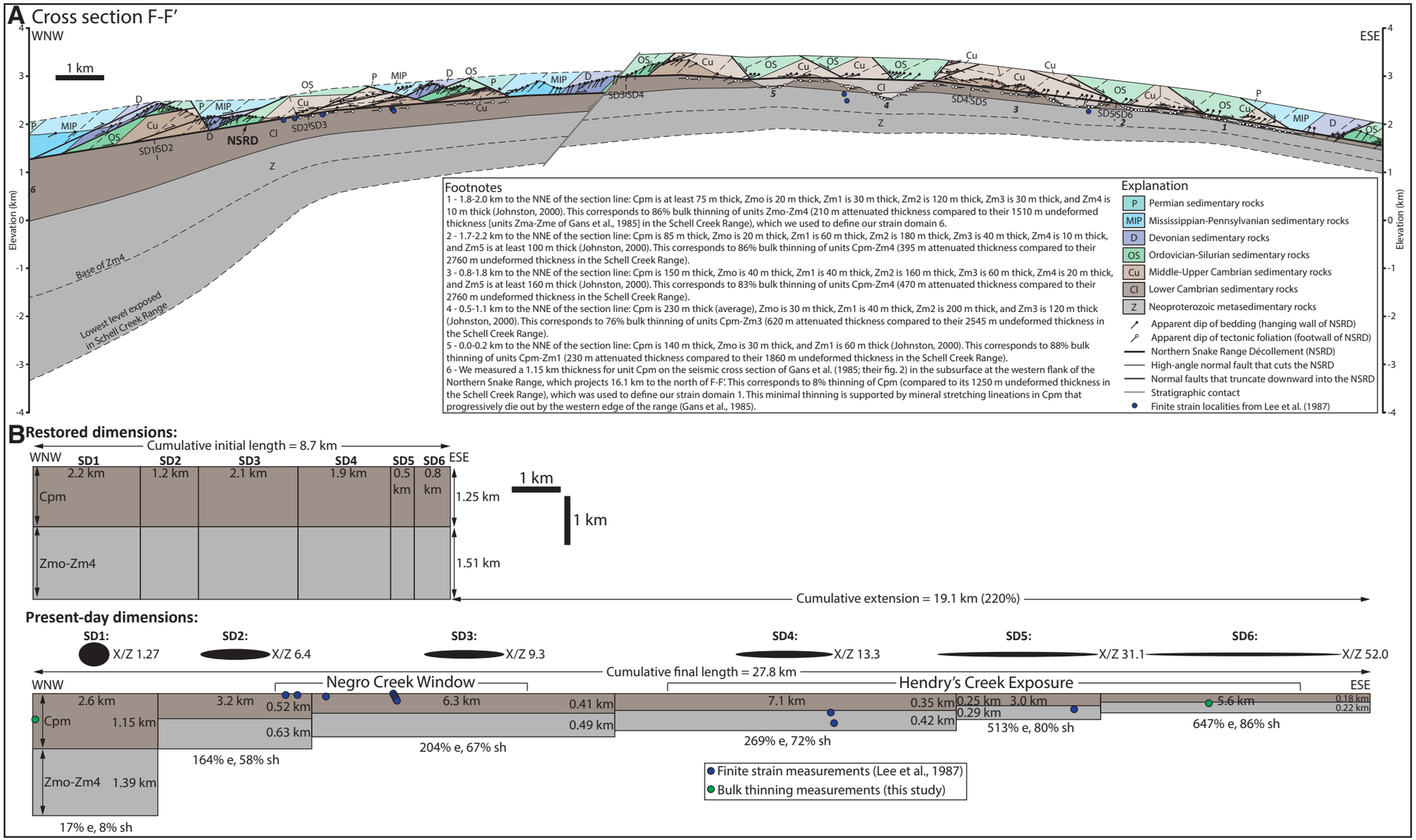

Figure 10. (A) Cross-section F-F′ through the Northern Snake Range, showing the present-day geometry (supported by the geologic map compilation of Johnston, 2000; line of section shown on Fig. 1B). Translucent areas above the modern surface represent eroded rock. Due to the complexity of normal faulting, rocks above the modern surface are only drafted as high as the minimum preserved structural height of rocks in the hanging wall of the Northern Snake Range décollement (NSRD) (0.7 km in the western part of the range, and 0.4 km in the central and eastern parts). Bold italic numbers are referenced to footnotes. SD—strain domain. (B) Six-domain model for finite strain in the footwall of the Northern Snake Range décollement along F-F′ showing restored dimensions (top diagram) and present-day dimensions (bottom diagram). Strain domains 2–5 were defined based on finite strain analyses from Lee et al. (1987), and strain domains 1 and 6 were defined based on measured attenuated thicknesses; see A for location of strain domains; see footnotes for A and Table 3 for details. Cpm—Lower Cambrian Prospect Mountain Quartzite; Zmo–Zm4—unit divisions of the Neoproterozoic McCoy Creek Group from Johnston (2000); e—lineation-parallel extension; sh—foliation-normal shortening.

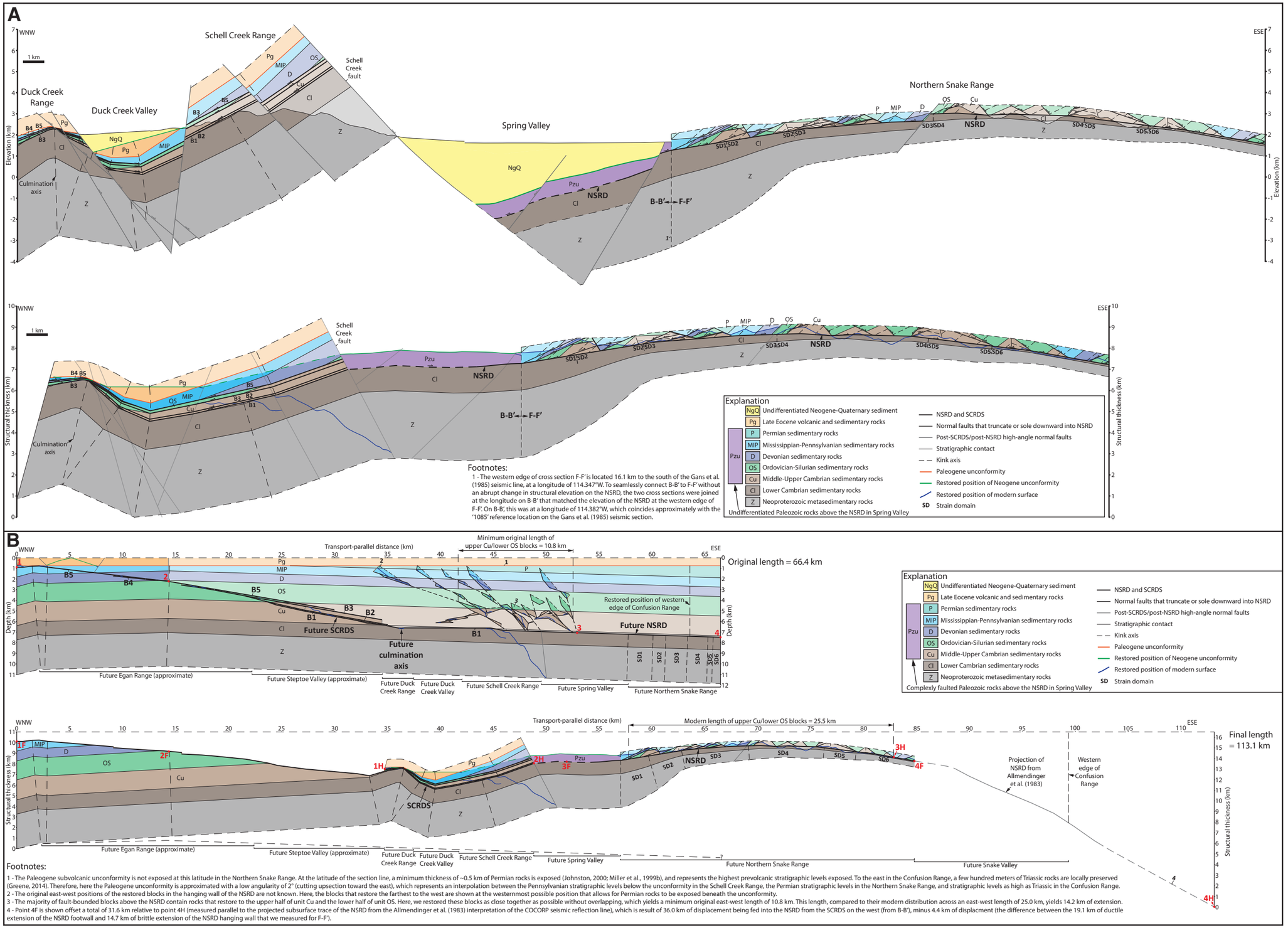

Figure 11. (A) Composite cross section across the Duck Creek, Schell Creek, and Northern Snake Ranges, consisting of B-B′ combined with F-F′ (lines of section shown on Fig. 1), which were joined at the longitude on B-B′ that matched the elevation of the Northern Snake Range décollement (NSRD) at the western edge of F-F′ (see footnote 1). The top cross section shows the present-day geometry, and the bottom cross section shows the geometry after retrodeformation of post–Schell Creek Range detachment system (SCRDS) faults (see footnotes and captions of Figs. 5 and 10). Bold italic numbers are referenced to footnotes. (B) Composite B-B′–F-F′ cross section (shown at a smaller size than A), showing a geometry that is restored for displacement on the linked Schell Creek Range detachment system–Northern Snake Range décollement fault system (SCRDS-NSRD; top cross section) and the post-SCRDS-NSRD geometry (bottom cross section; note that the geometry shown predates Neogene extension along high-angle Basin and Range normal faults). The restored section was drafted following published interpretations indicating that rocks in the Northern Snake Range décollement footwall restore to pre-extensional stratigraphic depths of ~7–12 km (Gans and Miller, 1983; Miller et al., 1983; Gans et al., 1985); we acknowledge that other pre-extensional geometries are possible (see text for discussion). Red numbers 1–4 on the restored section are displacement markers, and their corresponding positions in the footwall (F) and hanging wall (H) of the linked Schell Creek Range detachment system–Northern Snake Range décollement fault system are shown on the deformed cross section. The magnitude of isostatic uplift in rocks that restore to the west of the Duck Creek Range is schematic. COCORP—Consortium for Continental Reflection Profiling.

that many different pre-extensional geometries are possible, including those that allow for deeper structural burial of Northern Snake Range décollement footwall rocks (Bartley and Wernicke, 1984; Lewis et al., 1999; Cooper et al., 2010; Wrobel et al., 2021), and geometries that are compatible with interpretations that the Northern Snake Range décollement may have initiated at a moderate to steep (~40°) eastward dip angle (Lee, 1995). For this reason, our emphasis is on the implications of the extensional displacement magnitude along the Schell Creek Range detachment system that was fed eastward into the Northern Snake Range décollement. Given the assumptions above, we can use our pre-extensional geometry to postulate the magnitude of resulting brittle and ductile extension across the Northern Snake Range, although we regard the resulting extension values as approximate.

Geometry and Magnitude of Ductile and Brittle Extension in the Northern Snake Range

The Northern Snake Range décollement is exposed across the width of the Northern Snake Range (Figs. 1B and 10A). Above the Northern Snake Range décollement, Middle Cambrian to Permian sedimentary rocks were extended by two sets of top-down-to-the-ESE normal faults, including an older set of faults that have been rotated through horizontal to gentle westward dips by displacement and rotation along a younger set of high-angle normal faults (Miller et al., 1983; Johnston, 2000). All normal faults on cross-section F-F′ (with one exception) either terminate into or sole downward into the Northern Snake Range décollement (Fig. 10A), which is a top-down-to-the-ESE detachment surface that developed at the top of unit Cl (either within the Pioche Shale or at the top of the Prospect Mountain Quartzite; Miller et al., 1983). Beneath the Northern Snake Range décollement, Neoproterozoic to Lower Cambrian metasedimentary rocks have been ductilely stretched subhorizontally and thinned subvertically (Miller et al., 1983; Lee et al., 1987). All rocks in the Northern Snake Range décollement footwall exhibit a penetrative tectonic foliation that is subparallel to the décollement and ESE-trending mineral stretching lineations (Lee et al., 1987). The Northern Snake Range décollement has been broadly domed across the range (Fig. 10A), dipping ~10° on the range flanks and subhorizontal at the range crest.

Miller et al. (1983) documented that the magnitude of thinning of Neoproterozoic–Cambrian rocks in the Northern Snake Range décollement footwall increases moving eastward. This is best illustrated in unit Cl (the Prospect Mountain Quartzite), which has an approximately uniform thickness of 1.2–1.3 km in undeformed sections in ranges in the surrounding region (e.g., Young, 1960; Fritz, 1968; Hose and Blake, 1976; Gans and Miller, 1983; Miller et al., 1983; Lee et al., 1987; Rodgers, 1987; this study) but exhibits an attenuated thickness that decreases eastward to as little as ~100–200 m on the eastern flank of the Northern Snake Range (Miller et al., 1983). Lee et al. (1987) determined three-dimensional (3-D) finite strain ellipsoids from 11 localities in the Northern Snake Range décollement footwall, by measuring elongated detrital quartz grains and quartzite pebbles within the Prospect Mountain Quartzite and underlying Neoproterozoic quartzites. Their observations showed that bedding, tectonic foliation, the *x*-*y* strain plane, and the Northern Snake Range décollement are everywhere subparallel, and that 3-D strain was slightly constrictional (7% average shortening normal to lineation, with a total range of 0%–17%). They documented an eastward increase in lineation-parallel stretching at the latitude of cross section F-F′, which corroborates the field observation of increasing ductile thinning.

On cross section F-F′, we used the 11 finite strain analyses of Lee et al. (1987), combined with estimates of the ductile thinning magnitude of Neoproterozoic–Lower Cambrian rocks on the western and eastern flanks of the range, to generate a six-domain model for finite strain in the Northern Snake Range décollement footwall (Fig. 10B; Table 3). We divided the data of Lee et al. (1987) into four strain domains (abbreviated "SD") from west to east: SD2 has an average strain ellipsoid of 6.4:2.2:1.0 (n = 2), which corresponds to 164% lineation-parallel extension and 58% foliation-normal shortening; SD3 has an average ellipsoid of 9.3:3.1:1.0 (n = 6), which defines 204% extension and 67% shortening; SD4 has an average ellipsoid of 13.3:3.5:1.0 (n = 2), which corresponds to 270% extension and 72% shortening; and SD5 has a single ellipsoid of 31.1:4.2:1.0, which defines 513% extension and 80% shortening. We defined two additional strain domains, one on the western flank of the range (SD1), where the thickness of the Prospect Mountain Quartzite on the interpreted seismic cross section of Gans et al. (1985) defines 8% bulk thinning (Fig. 10A, footnote 6), and one on the eastern flank of the range (SD6), where attenuated thicknesses on cross-section F-F′ define 86% bulk thinning of the Prospect Mountain Quartzite and underlying Neoproterozoic units (Fig. 10A, footnote 1). Using these thinning magnitudes, and assuming 7% lineation-normal shortening for these two strain domains (which is the average of the four strain domains defined by the data of Lee et al., 1987), we calculated an ellipsoid of 1.27:1.02:1.00 for SD1, defining 17% extension and 8% shortening, and an ellipsoid of 52.0:6.5:1.0 for SD6, corresponding to 647% extension and 86% shortening. The low strain magnitude for SD1 is corroborated by stretching lineations in the Prospect Mountain Quartzite that progressively die out toward the northwestern flank of the range (Gans et al., 1985; Lee et al., 1999b). The six strain domains have a cumulative modern WNW-ESE length of 27.8 km. Restoration of the strain domains to their undeformed geometry defines an original length of 8.7 km, corresponding to 19.1 km of cumulative extension (220%) via ductile stretching (Fig. 10B), which is similar to the 250% estimate obtained by Lee et al. (1987).

Measuring the magnitude of brittle extension above the Northern Snake Range décollement along cross-section F-F′ is more difficult, as the restored east-west positions of the preserved fault-bounded blocks in its hanging wall cannot be easily constrained. Using the geologic map compilation of Johnston (2000), we performed three-point problems (n = 25) on normal faults on cross-section F-F′ (supporting data in Table S5), which demonstrated that the older set of rotated, west-dipping normal faults generally dip between 13° and 24°W (19°W average) and exhibit stratigraphic cutoff angles typically between

TABLE 3. SUPPORTING DATA FOR THE SIX-DOMAIN FINITE STRAIN MODEL FOR THE NORTHERN SNAKE RANGE DÉCOLLEMENT FOOTWALL FOR CROSS-SECTION F-F′ (SEE FIG. 10B)

Strain domain	Number of supporting finite strain analyses from Lee et al. (1987)	Average *X*/*Z*	Average *Y*/*Z*	Average *Z*	Undeformed sphere diameter	Lineation-parallel (*X*) extension (%)	Lineation-normal (*Y*) extension (%)	Foliation-normal (*Z*) shortening (%)	Modern east-west length (km)	Undeformed thickness (Cpm) (km)	Undeformed thickness (Zmo-Zm4) (km)	Modern thickness (Cpm) (km)	Modern thickness (Zmo–Zm4) (km)	Restored east-west length (km)	Extension (km)
1	*	1.27	1.02	1.0	1.09	17	–7	8	2.6	1.25	1.51	1.15	1.39	2.23	0.4
2	2 (JL1-115, 116)	6.4	2.2	1.0	2.41	164	–9	58	3.2	1.25	1.51	0.52	0.63	1.21	2.0
3	6 (JL1-148, 149, 150, 151, 152, 157)	9.3	3.1	1.0	3.05	204	0	67	6.3	1.25	1.51	0.41	0.49	2.07	4.2
4	2 (JL2-32, SP4)	13.3	3.5	1.0	3.59	269	–3	72	7.1	1.25	1.51	0.35	0.42	1.93	5.2
5	1 (JL2-91)	31.1	4.2	1.0	5.07	513	–17	80	3.0	1.25	1.51	0.25	0.29	0.49	2.5
6	†	52.0	6.5	1.0	6.97	647	–7	86	5.6	1.25	1.51	0.18	0.22	0.75	4.8

Note: Cpm is the Prospect Mountain Quartzite, and units Zmo–Zm4 are unit divisions of the Neoproterozoic McCoy Creek Group from Johnston (2000), which are correlated with units Zma–Zme of Gans et al. (1985) on B-B′.

*Strain domain 1: We generated a strain ellipsoid that yielded 8% vertical thinning (based on the 1.15 km thickness of Cpm measured in the subsurface under the western flank of the northern Snake Range on the seismic cross section of Gans et al. [1985], compared to its 1.25 km undeformed thickness in surrounding ranges), assuming –7% *Y* extension (the average for strain domains 2–5).

†Strain domain 6: We generated a strain ellipsoid that yielded 86% vertical thinning (based on the 210 m attenuated thickness of units Zmo–Zm4 on the eastern end of F-F′, compared to their 1.51 km undeformed thickness in the Schell Creek Range), assuming –7% *Y* extension (the average for strain domains 2–5).

13° and 27° (20° average). The younger set of east-dipping faults typically dip between 27° and 47°E (32°E average) and have highly variable cutoff angles. The majority of fault-bounded blocks on cross-section F-F′ contain Middle–Upper Cambrian to Ordovician rocks (Fig. 10A). By restoring these blocks of units Cu and OS as close together as possible without overlapping, we measured a minimum original east-west length of 10.8 km (Fig. 11B). When compared to their present-day distribution across an east-west length of 25.5 km, this defines 14.7 km of extension (136%). This estimate should be considered approximate, as it does not account for restoration of faults that carry the more sparsely preserved Devonian–Permian rocks. However, this is similar to published estimates of brittle extension above the Northern Snake Range décollement, which range from 13 to 25 km (Miller et al., 1983; Long, 2019).

Overlap in Timing of Displacement along the Schell Creek Range Detachment System and Northern Snake Range Décollement

The timing of displacement along the Schell Creek Range detachment system and the Northern Snake Range décollement overlaps between the late Eocene and late Oligocene. The timing of extension in the Northern Snake Range was recently summarized by Lee et al. (2017), and readers are referred to their study for a detailed discussion. Normal fault–related tilting in the Northern Snake Range décollement hanging wall initiated as early as ca. 35 Ma and continued until at least ca. 24–21 Ma (Gans et al., 1989; Martinez et al., 1998), and dating of undeformed and deformed rhyolitic dikes that intrude the Northern Snake Range décollement footwall brackets high-strain ductile stretching and mylonitization between ca. 37.8 Ma and ca. 22.5 Ma (Lee et al., 2017). This timing range is supported by thermochronometry data (muscovite and K-feldspar $^{40}Ar/^{39}Ar$, zircon fission track) from rocks in the Northern Snake Range décollement footwall that define an eastward-younging cooling history, which has been interpreted to represent the progressive migration of synextensional exhumational unroofing (Lee and Sutter, 1991; Lee, 1995; Miller et al., 1999a; Gébelin et al., 2011). Apatite fission-track ages from the Northern Snake Range décollement footwall require that extension-related cooling continued until at least ca. 17–15 Ma (Miller et al., 1999a). However, this late-stage extension postdated the ductile stretching of the Northern Snake Range décollement footwall and was likely related to a younger, regionally pervasive episode of high-angle Basin and Range normal faulting (Gans et al., 1985; Lee et al., 2017).

Top-down-to-the-ESE extension along the Schell Creek Range detachment system is bracketed between ca. 36.5 and 26.1 Ma (see section Constraints on the Timing of Extension on the Schell Creek Range Detachment System), which falls within the ca. 37.8–22.5 Ma bracketed timing range for ductile stretching of the Northern Snake Range décollement footwall (Lee et al., 2017) and is compatible with the ca. 35 Ma initiation of normal faulting in the Northern Snake Range décollement hanging wall (Gans et al., 1989).

Geometric Model for the Linked Schell Creek Range Detachment System–Northern Snake Range Décollement Extensional System

The Schell Creek Range detachment system and the Northern Snake Range décollement both accommodated high-magnitude, top-down-to-the-ESE extension, and the timing of displacement along these detachment systems overlapped. These observations, combined with their spatial proximity (their map traces are separated today by as little as ~17 km E-W distance, which reduces to as little as ~10 km after restoration of post–Schell Creek Range

detachment system normal faulting; Fig. 5) and the similar stratigraphic level to which they root (the top of the Lower Cambrian clastic section), lead us to interpret that they represent the western (Schell Creek Range detachment system) and eastern (Northern Snake Range décollement) components of the same integrated fault system (illustrated by combining cross-sections B-B′ and F-F′ on Fig. 11A). We suggest that the Schell Creek Range detachment system represents the low-angle breakaway zone, which traversed the upper ~7 km of the crust at an average cutoff angle of ~10° (Fig. 11B). The Schell Creek Range detachment system rooted eastward to a flat at the top of the Lower Cambrian clastic section, which accommodated polyphase brittle extension in its hanging wall and a progressively eastward-increasing component of ductile stretching in its footwall and is expressed today as the Northern Snake Range decollement. With progressive extension and isostatic rebound, the Schell Creek Range detachment system evolved via repeated excision into an imbricate stack of thin sheets that are folded across a narrow anticlinal culmination (Fig. 4D).

The minimal angularity of the Paleogene unconformity in the Schell Creek and Duck Creek Ranges (Young, 1960; Drewes, 1967; Gans and Miller, 1983), when combined with the stratigraphic levels and low stratigraphic cutoff angles of Schell Creek Range detachment faults, constrains the shallow crustal depth and gentle initial eastward dip of the detachment system in the western ~8 km of our restored section (Fig. 11B). However, due to uncertainties in the pre-extensional geometry of the Northern Snake Range (e.g., Miller et al., 1983; Bartley and Wernicke, 1984; Lewis et al., 1999; Cooper et al., 2010; Hoiland, 2019; Wrobel et al., 2021), the initial dip angle of the eastern portion of the Schell Creek Range detachment system is less certain. Our reconstruction (Fig. 11B), which restores rocks in the Northern Snake Range décollement footwall to their original stratigraphic depths (after Miller et al., 1983), and which shows the Schell Creek Range detachment system dipping ~10°E and rooting to a flat at the top of the Lower Cambrian section, can be considered an end-member geometry that yields the lowest initial dip angle. However, published barometry and structural reconstructions argue that the pre-extensional depths of the Northern Snake Range décollement footwall may have been deeper (Cooper et al., 2010; Wrobel et al., 2021), which could increase the initial dip angle of the eastern portion of the Schell Creek Range detachment system. Assuming a homogeneous eastward dip for the Northern Snake Range décollement and the eastern portion of the Schell Creek Range detachment system, the ~7 km of structural burial via folding that Wrobel et al. (2021) argued for in the northern part of the Northern Snake Range would yield in an average dip of ~13°E. Peak pressure estimates from two Neoproterozoic samples collected proximal to the eastern edge of our F-F′ cross-section line by Cooper et al. (2010) (sample FHe9: 5.7 ± 0.9 kbar, and sample FHe268: 6.1 ± 0.7 kbar) would yield an initial dip range between ~14° and 21°E (assuming a lithostatic gradient of ~3.7 kbar/km). However, we emphasize that the initial dip angle of the Northern Snake Range décollement and the eastern portion of the Schell Creek Range detachment system does not affect the stratigraphic cutoff angles or displacement estimates that we calculated in our cross-section reconstructions.

Under our interpretation of a linked Schell Creek Range detachment system–Northern Snake Range décollement fault system, the cumulative displacement on the Schell Creek Range detachment system that we measured provides an important new constraint on the magnitude of displacement on the Northern Snake Range décollement, which has been the subject of long-standing debate (e.g., Gans and Miller, 1983; Miller et al., 1983; Bartley and Wernicke, 1984; Gans et al., 1985; Lee et al., 1987; Lewis et al., 1999; Cooper et al., 2010). For example, Miller et al. (1983) argued that large-magnitude displacement on the Northern Snake Range décollement was not required because of the lack of stratigraphic omission across the detachment fault and the similar magnitudes of ductile extension in the footwall and brittle extension in the hanging wall. In contrast, other studies have argued for as much as 60 km of displacement along the Northern Snake Range décollement (Bartley and Wernicke, 1984).

To estimate the magnitude of extension accommodated by a linked Schell Creek Range detachment system–Northern Snake Range décollement fault system, we show present-day and restored versions of our combined B-B′–F-F′ cross section (Fig. 11B). Even though the 19.1 km of ductile stretching of the Northern Snake Range décollement footwall exceeded the 14.7 km of brittle extension of the Northern Snake Range décollement hanging wall, the 36.0 km of total displacement on the Schell Creek Range detachment system, which was fed into the Northern Snake Range décollement from the west, would require significant differential displacement between the footwall and hanging wall of the Northern Snake Range décollement. At the minimum (because we do not account for any extension that may have been accommodated in the Paleozoic rocks above the Northern Snake Range décollement in Spring Valley, interpreted on the seismic cross section of Gans et al., 1985), 31.6 km of the 36.0 km of displacement fed into the Northern Snake Range décollement from the Schell Creek Range detachment system must have been translated east of the eastern flank of the Northern Snake Range (calculated by subtracting the 4.4 km of differential extension between the Northern Snake Range décollement footwall and hanging wall from the 36.0 km total Schell Creek Range detachment system displacement fed eastward into the Northern Snake Range décollement; Fig. 11B, footnote 4 of that figure). Therefore, though displacement at any given point on the Northern Snake Range décollement will vary (e.g., depending on the strain domain in which it lies and the stratigraphic level of the hanging wall), our reconstruction defines at least 31.6 km of top-down-to-the-ESE displacement at its eastern exposed extent.

The restored cross section on Figure 11B has an initial length of 66.4 km between the western limit of rocks exposed in the Duck Creek Range (red point 1) and the eastern limit of exposure of the Northern Snake Range décollement footwall (red point 4). On the deformed cross section on Figure 11B, we drafted the ~30°E-dipping subsurface interpretation of the Northern Snake Range décollement from the COCORP seismic reflection profile (Allmendinger et al., 1983). Projection of 31.6 km of displacement on the subsurface trace of the Northern Snake Range décollement (red points 4F and 4H) yields a final length of 113.1 km, which defines 46.7 km of minimum extension accommodated by the linked Schell Creek Range detachment system–Northern Snake Range décollement

fault system (calculated by subtracting the 66.4 km initial length from the 113.1 km final length). However, we view this cumulative extension estimate as approximate, as we acknowledge that a range of pre-extensional geometries for the Northern Snake Range is possible based on different interpretations of the origination angle of the Northern Snake Range décollement and the burial depths of rocks in its footwall (Miller et al., 1983; Bartley and Wernicke, 1984; Gans et al., 1985; Lee, 1995; Lewis et al., 1999; Cooper et al., 2010; Hoiland, 2019; Long, 2019; Wrobel et al., 2021; see discussion in Geometry and Magnitude of Ductile and Brittle Extension in the Northern Snake Range section).

Implications for Regional Extension in Eastern Nevada

The Northern Snake, Schell Creek, and Duck Creek Ranges, as well as the Egan Range to the west, lie within a NNE-trending, ~120-km-wide (present-day dimensions) domain of high-magnitude mid-Cenozoic extension (Gans and Miller, 1983; Axen et al., 1993), and the Schell Creek Range detachment system–Northern Snake Range décollement was the master extensional fault system at this latitude. The restored geometry on Figure 11B implies that the Schell Creek Range detachment system also deformed rocks that today lie in the Egan Range. Exposures in the Egan Range at this latitude are dominated by complexly extended Mississippian to Permian rocks and Eocene volcanic rocks (e.g., Hose and Blake, 1976), and thus they may represent allochthonous rocks translated eastward above the basal fault of the Schell Creek Range detachment system. This is compatible with geologic mapping in the Egan Range west of the area of Figure 1C that defined several N-striking faults with low stratigraphic cutoff angles that can be correlated for map distances up to 20 km, including the Chainman and Upper Bench faults, which omit Mississippian and Pennsylvanian stratigraphy, and the Kaibab fault, which omits Permian stratigraphy (Brokaw and Shaw, 1965; Brokaw and Heidrick, 1966; Brokaw, 1967; Brokaw and Barosh, 1968; Brokaw et al., 1973). At the latitude of cross-section C-C′, Gans et al. (2001) documented synvolcanic extension between 37.6 and 36.7 Ma in the Egan Range, which is similar to the timing range for the Schell Creek Range detachment system.

South of our studied latitude, extension along low-angle detachment systems was the dominant deformation style. Ninety kilometers to the southwest, the top-down-to-the-west Grant Range detachment system accommodated 24–49 km of extension between ca. 31 and 15 Ma and is similar in structural style to the Schell Creek Range detachment system (Lund et al., 1993; Camilleri, 2013; Long and Walker, 2015; Long et al., 2018). About 110 km to the south, the top-down-to-the-east Stampede detachment system accommodated extension between ca. 34 and 30 Ma (Axen et al., 1988, 1993; Taylor et al., 1989; Taylor, 1990), and it has been interpreted to correlate with the Northern Snake Range décollement (Taylor and Bartley, 1992).

To the north (~20–50 km N of the latitude of cross-section A-A′), a transition in style to high-angle, domino-style normal faults that cut down to ~10–15 km depths without flattening is observed in the Egan, Cherry Creek, and Deep Creek Ranges (Fritz, 1968; Wernicke, 1981; Gans, 1982; Gans and Miller, 1983; Rodgers, 1987; Blackford et al., 2022). No extension estimates are available for the Schell Creek Range at this latitude, but Blackford et al. (2022) measured 28.1 km of extension across the Deep Creek Range and 15.8 km across the Egan and Cherry Creek Ranges, indicating at least 43.9 km of extension at this latitude, which is similar to our 46.7 km approximate extension estimate for the linked Schell Creek Range detachment system–Northern Snake Range décollement.

Displacement on the Schell Creek Range detachment system between ca. 37 and 26 Ma provides another example of mid-Cenozoic extension via low-dip-angle, brittle detachment faulting in eastern Nevada, which also included the ca. 31–15 Ma Grant Range detachment system (Lund et al., 1993; Camilleri, 2013; Long and Walker, 2015; Long et al., 2018) and the ca. 34–30 Ma Stampede detachment system (Axen et al., 1988, 1993; Bartley et al., 1988; Taylor, 1990; Taylor and Bartley, 1992). This early phase of regional extension was likely promoted by several factors, including the reduction of interplate coupling that accompanied post-Laramide rollback of the Farallon slab, crustal heating during the associated Great Basin ignimbrite flare-up, and the thick crust of the Cordilleran retroarc (e.g., Dickinson and Snyder, 1978; Humphreys, 1995; Dickinson, 1991, 2004, 2006; Smith et al., 2014; Long et al., 2018). Rotation of the upper-crustal stress field to an orientation favorable for low-angle brittle extensional faulting may have been the consequence of shear traction imparted to the base of the brittle crust by lower-crustal flow that accompanied initial extension of the thick Cordilleran retroarc crust (e.g., Yin, 1989; Harry et al., 1993; Westaway, 1999).

Implications for the Style of Hanging-Wall Deformation above Detachment Fault Systems

Most models for extension in the hanging wall of an actively slipping, low-angle detachment fault system depict arrays of closely spaced, initially high angle, planar or listric normal faults, which rotate to shallower dips with progressive extension (e.g., Davis et al., 1980; Wernicke, 1981; Wernicke and Burchfiel, 1982; Chamberlin, 1983; Jackson and McKenzie, 1983; Lister et al., 1986), and this geometry is exemplified by the normal faulting in the hanging wall of the Northern Snake Range décollement (e.g., Miller et al., 1983). However, the Schell Creek Range detachment system breakaway zone exhibits as many as five structurally intact, detachment-bounded sheets that are as long as ~8–13 km in the transport direction, which lack evidence for any internal deformation by high-angle normal faults that truncate downward or sole into Schell Creek Range detachment faults. This contrasts with other detachment fault systems that record excision, including the Bannock detachment system in Idaho (Carney and Janecke, 2005; Steely et al., 2005) and the Whipple Mountains detachment system in California (Davis et al., 1980, 1986; Lister and Davis, 1989; Yin and Dunn, 1992), which exhibit multiple high-angle normal faults that truncate downward into low-angle detachment faults and are interpreted as listric faults that have had their basal portions "beheaded" by excision. The geometry of the Schell Creek Range detachment system demonstrates that a significant thickness of the hanging wall (at least an

~1.0–1.5 km structural thickness, based on the cumulative preserved thicknesses of restored sheets on cross-sections A-A′ and B-B′ on Fig. 4) above an actively slipping low-angle detachment fault surface can remain structurally intact, even during slip at shallow crustal depths.

CONCLUSIONS

(1) The Schell Creek Range detachment system consists of a series of top-down-to-the-ESE brittle normal faults that traversed the upper ~7 km of the crust at an ~5°–10°E initial dip and rooted eastward to a flat at the top of the Lower Cambrian clastic section. The Schell Creek Range detachment system evolved through progressive excision to produce an upward-younging stack of 0.1–0.5-km-thick, fault-bounded sheets that are up to 8–13 km long. The western part of the Schell Creek Range detachment system was folded across an antiformal culmination and exhibits ~5 km of structural attenuation. The Schell Creek Range detachment system accommodated at least 36 km of ESE-directed displacement between ca. 36.5 and ca. 26.1 Ma.

(2) Based on their spatial proximity, displacement sense, overlapping deformation timing, and the shared stratigraphic level that they root to, we propose that the Schell Creek Range detachment system is the western breakaway zone for the Northern Snake Range décollement. Unresolved debates over the initial geometry of the Northern Snake Range décollement hinder accurate estimation of cumulative extension on the linked Schell Creek Range detachment system–Northern Snake Range décollement fault system, but our reconstruction indicates that at least 36 km of displacement was fed eastward into the Northern Snake Range décollement from extension along the Schell Creek Range detachment system.

(3) The linked Schell Creek Range detachment system–Northern Snake Range décollement was the dominant fault system within a domain of high-magnitude, mid-Cenozoic extension in eastern Nevada. Extension along low-angle detachment systems was the dominant style further to the south in this domain, but to the north, the style transitioned to high-angle, domino-style normal faults that cut as deep as 10–15 km without flattening.

(4) Our study supports the existence of extensive (>50 km map length), low-dip-angle (~10°), shallow-crustal (1–7 km depths), brittle detachment faults, and demonstrates that portions of their hanging walls can remain structurally intact during displacement.

ACKNOWLEDGMENTS

This work was supported by National Science Foundation (NSF) grant EAR-2022973 awarded to S. Long and NSF grant EAR-2022979 awarded to J. Lee. Several of the ideas presented here were inspired by the research of many outstanding geologists who have worked in the Basin and Range Province, including Ernest Anderson, Elizabeth Miller, Phil Gans, Brian Wernicke, Gordon Lister, Jim Faulds, Susanne Janecke, and Andrew Zuza. We thank Associate Editor Andrew Zuza, reviewer Brandon Lutz, and an anonymous reviewer for their constructive comments that significantly improved this paper. The article and supplemental material contain all of the data used for this research.

REFERENCES CITED

Allmendinger, R.W., 1992, Fold and thrust tectonics of the western United States exclusive of the accreted terranes, *in* Burchfiel, B.C., et al., eds., The Cordilleran Orogen: Conterminous U.S.: Boulder, Colorado, Geological Society of America, Geology of North America, v. G-3, p. 583–608, https://doi.org/10.1130/DNAG-GNA-G3.583.

Allmendinger, R.W., Sharp, J.W., Von Tish, D., Serpa, L., Brown, L., Kaufman, S., and Oliver, J., 1983, Cenozoic and Mesozoic structure of the eastern Basin and Range Province, Utah, from COCORP seismic-reflection data: Geology, v. 11, p. 532–536, https://doi.org/10.1130/0091-7613(1983)11<532:CAMSOT>2.0.CO;2.

Anderson, E.R., 1983, Cenozoic structural history of selected areas in the eastern Great Basin, Nevada-Utah: U.S. Geological Survey Open-File Report 83-504, https://doi.org/10.3133/ofr83504.

Armstrong, R.L., 1968, Sevier orogenic belt in Nevada and Utah: Geological Society of America Bulletin, v. 79, p. 429–458, https://doi.org/10.1130/0016-7606(1968)79[429:SOBINA]2.0.CO;2.

Armstrong, R.L., 1972, Low-angle (denudation) faults, hinterland of the Sevier orogenic belt, eastern Nevada and western Utah: Geological Society of America Bulletin, v. 83, p. 1729–1754, https://doi.org/10.1130/0016-7606(1972)83[1729:LDFHOT]2.0.CO;2.

Axen, G.J., Lewis, K.J., Burke, K.J., Sleeper, K.G., and Fletcher, J.M., 1988, Tertiary extension in the Pioche area, Nevada, *in* Weide, D.L., and Faber, M.L., eds., This Extended Land, Geological Journeys in the Southern Basin and Range: Cordilleran Section Field Trip Guidebook: Las Vegas, Nevada, University of Nevada–Las Vegas, and Geological Society of America, p. 3–5.

Axen, G.J., Taylor, W.J., and Bartley, J.M., 1993, Space-time patterns and tectonic controls of Tertiary extension and magmatism in the Great Basin of the western United States: Geological Society of America Bulletin, v. 105, p. 56–76, https://doi.org/10.1130/0016-7606(1993)105<0056:STPATC>2.3.CO;2.

Bartley, J.M., and Wernicke, B.P., 1984, The Snake Range décollement interpreted as a major extensional shear zone: Tectonics, v. 3, p. 647–657, https://doi.org/10.1029/TC003i006p00647.

Bartley, J.M., Axen, G.J., Taylor, W.J., and Fryxell, J.E., 1988, Cenozoic tectonics of a transect through eastern Nevada near 38°N latitude, *in* Weide, D.L., and Faber, M.L., eds., This Extended Land: Geological Journeys in the Southern Basin and Range: Geological Society of America, Cordilleran Section, Field Trip Guidebook: Las Vegas, Nevada, Department of Geoscience, University of Nevada, p. 1–20.

Barton, M.D., 1990, Cretaceous magmatism, metamorphism, and metallogeny in the east-central Great Basin, *in* Anderson, J.L., ed., The Nature and Origin of Cordilleran Magmatism: Geological Society of America Memoir 174, p. 283–302, https://doi.org/10.1130/MEM174-p283.

Blackford, N.R., Long, S.P., Stout, A.J., Rodgers, D.W., Cooper, C.M., Kramer, K., Di Fiori, R.V., and Soignard, E., 2022, Late Cretaceous upper-crustal thermal structure of the Sevier hinterland: Implications for the geodynamics of the Nevadaplano: Geosphere, v. 18, p. 183–210, https://doi.org/10.1130/GES02386.1.

Brokaw, A.L., 1967, Geologic Map and Sections of the Ely Quadrangle, White Pine County, Nevada: U.S. Geological Survey Geologic Quadrangle Map GQ-697, scale 1:24,000, 1 plate, https://doi.org/10.3133/gq697.

Brokaw, A.L., and Barosh, P.J., 1968, Geologic Map of the Riepetown Quadrangle, White Pine County, Nevada: U.S. Geological Survey Geologic Quadrangle Map GQ-758, scale 1:24,000, 1 plate, https://doi.org/10.3133/gq758.

Brokaw, A.L., and Heidrick, T., 1966, Geologic Map and Sections of the Giroux Wash Quadrangle, White Pine County, Nevada: U.S. Geological Survey Geologic Quadrangle Map GQ-476, scale 1:24,000, 1 plate, https://doi.org/10.3133/gq476.

Brokaw, A.L., and Shaw, D.R., 1965, Geologic Map and Sections of the Ely 3 SW Quadrangle, White Pine County, Nevada: U.S. Geological Survey Miscellaneous Geologic Investigations Map I-449, scale 1:24,000, 1 plate, https://doi.org/10.3133/i449.

Brokaw, A.L., Bauer, H.L., and Breitrick, R.A., 1973, Geologic Map of the Ruth Quadrangle, White Pine County, Nevada: U.S. Geological Survey Geologic Quadrangle Map GQ-1085, scale 1:24,000, 1 plate, https://doi.org/10.3133/gq1085.

Buck, W.R., 1991, Modes of continental lithospheric extension: Journal of Geophysical Research, v. 96, p. 20,161–20,178, https://doi.org/10.1029/91JB01485.

Camilleri, P.A., 2013, Geologic Map and Structure of the West-Central Part of the Grant Range, Nye County, Nevada: Geological Society of America Digital Map and Chart Series 14, 25 p., https://doi.org/10.1130/2013.DMCH014.

Carney, S.M., and Janecke, S.U., 2005, Excision and the original low dip of the Miocene–Pliocene Bannock detachment system, SE Idaho: Northern cousin of the Sevier Desert detachment?: Geological Society of America Bulletin, v. 117, p. 334–353, https://doi.org/10.1130/B25428.1.

Cassel, E.J., Breecker, D.O., Henry, C.D., Larson, T.E., and Stockli, D.F., 2014, Profile of a paleo-orogen: High topography across the present-day Basin and Range from 40 to 23 Ma: Geology, v. 42, p. 1007–1010, https://doi.org/10.1130/G35924.1.

Chamberlin, R.M., 1983, Cenozoic domino-style crustal extension in the Lemitar Mountains, New Mexico: A summary, *in* Chapin, C.E., and Callender, J.F., eds., Guidebook for the 34th Field Conference, Socorro Region II: Socorro, New Mexico, New Mexico Geological Society, p. 111–118.

Chapman, J.B., Ducea, M.N., DeCelles, P.G., and Profeta, L., 2015, Tracking changes in crustal thickness during orogenic evolution with Sr/Y: An example from the North American Cordillera: Geology, v. 43, p. 919–922, https://doi.org/10.1130/G36996.1.

Colgan, J.P., and Henry, C.D., 2009, Rapid middle Miocene collapse of the Mesozoic orogenic plateau in north-central Nevada: International Geology Review, v. 51, p. 920–961, https://doi.org/10.1080/00206810903056731.

Coney, P.J., 1974, Structural analysis of the Snake Range décollement, east-central Nevada: Geological Society of America Bulletin, v. 85, p. 973–978, https://doi.org/10.1130/0016-7606(1974)85<973:SAOTSR>2.0.CO;2.

Coney, P.J., and Harms, T., 1984, Cordilleran metamorphic core complexes: Cenozoic extensional relics of Mesozoic compression: Geology, v. 12, p. 550–554, https://doi.org/10.1130/0091-7613(1984)12<550:CMCCCE>2.0.CO;2.

Cooper, F.J., Platt, J.P., Anczkiewicz, R., and Whitehouse, J., 2010, Footwall dip of a core complex detachment fault: Thermobarometric constraints from the northern Snake Range (Basin and Range, USA): Journal of Metamorphic Geology, v. 28, p. 997–1020, https://doi.org/10.1111/j.1525-1314.2010.00907.x.

Crittenden, M.D., Jr., Coney, P.J., and Davis, G.H., eds., 1980, Cordilleran Metamorphic Core Complexes: Geological Society of America Memoir 153, 490 p., https://doi.org/10.1130/MEM153-p485.

Davis, G.A., Anderson, J.L., Frost, E.G., and Shackelford, T.J., 1980, Mylonitization and detachment faulting in the Whipple-Buckskin-Rawhide Mountains terrane, southeastern California, and western Arizona, *in* Crittenden, M.D., Jr., Coney, P.J., and Davis, G.H., eds., Cordilleran Metamorphic Core Complexes: Geological Society of America Memoir 153, p. 79–130, https://doi.org/10.1130/MEM153-p79.

Davis, G.A., Lister, G.S., and Reynolds, S.J., 1986, Structural evolution of the Whipple and South Mountains shear zones, southwestern United States: Geology, v. 14, p. 7–10, https://doi.org/10.1130/0091-7613(1986)14<7:SEOTWA>2.0.CO;2.

DeCelles, P.G., 2004, Late Jurassic to Eocene evolution of the Cordilleran thrust belt and foreland basin system, western U.S.A.: American Journal of Science, v. 304, p. 105–168, https://doi.org/10.2475/ajs.304.2.105.

Dechert, C.P., 1967, Bedrock Geology of the Northern Schell Creek Range, White Pine County, Nevada [Ph.D. dissertation]: Seattle, Washington, University of Washington, 266 p.

Dewey, J.F., 1988, Extensional collapse of orogens: Tectonics, v. 7, p. 1123–1139, https://doi.org/10.1029/TC007i006p01123.

Dickinson, W.R., 1991, Tectonic setting of faulted Tertiary strata associated with the Catalina core complex in southern Arizona: Geological Society of America Special Paper 264, 106 p.

Dickinson, W.R., 2002, The Basin and Range Province as a composite extensional domain: International Geology Review, v. 44, p. 1–38, https://doi.org/10.2747/0020-6814.44.1.1.

Dickinson, W.R., 2004, Evolution of the North American Cordillera: Annual Review of Earth and Planetary Sciences, v. 32, p. 13–45, https://doi.org/10.1146/annurev.earth.32.101802.120257.

Dickinson, W.R., 2006, Geotectonic evolution of the Great Basin: Geosphere, v. 2, p. 353–368, https://doi.org/10.1130/GES00054.1.

Dickinson, W.R., and Snyder, W.S., 1978, Plate tectonics of the Laramide orogeny, *in* Mathews, V., III, ed., Laramide Folding Associated With Basement Block Faulting in the Western United States: Geological Society of America Memoir 151, p. 355–366, https://doi.org/10.1130/MEM151-p355.

Dilek, Y., and Moores, E.M., 1999, A Tibetan model for the early Tertiary western United States: Journal of the Geological Society [London], v. 156, p. 929–941, https://doi.org/10.1144/gsjgs.156.5.0929.

Drewes, H., 1967, Geology of the Connors Pas Quadrangle, Schell Creek Range, East-Central Nevada: U.S. Geological Survey Professional Paper 557, scale 1:48,000, 1 sheet, 97 p., https://doi.org/10.3133/pp557.

Druschke, P., Hanson, A.D., and Wells, M.S., 2009, Structural, stratigraphic, and geochronologic evidence for extension predating Palaeogene volcanism in the Sevier hinterland, east-central Nevada: International Geology Review, v. 51, p. 743–775, https://doi.org/10.1080/00206810902917941.

Druschke, P., Hanson, A.D., Wells, M.L., Gehrels, G.E., and Stockli, D., 2011, Paleogeographic isolation of the Cretaceous to Eocene Sevier hinterland, east-central Nevada: Insights from U-Pb and (U-Th)/He detrital zircon ages of hinterland strata: Geological Society of America Bulletin, v. 123, p. 1141–1160, https://doi.org/10.1130/B30029.1.

Fouch, T.D., Hanley, J.M., and Forester, R.M., 1979, Preliminary correlation of Cretaceous and Paleogene lacustrine and related nonmarine sedimentary and volcanic rocks in parts of the Great Basin of Nevada and Utah, *in* Newman, G.W., and Goode, H.D., eds., Basin and Range Symposium and Great Basin Field Conference: Denver, Colorado, Rocky Mountain Association of Petroleum Geologists and Utah Geological Association, p. 305–312.

Fritz, W.H., 1968, Geologic Map and Sections of the Southern Cherry Creek and Northern Egan Ranges, White Pine County, Nevada: Nevada Bureau of Mines and Geology Map 35, scale 1:62,500, 1 plate, https://data.nbmg.unr.edu/public/freedownloads/m/m035.zip.

Gans, P.B., 1982, Mid-Tertiary Magmatism and Extensional Faulting in the Hunter District, White Pine County, Nevada [Ph.D. dissertation]: Palo Alto, California, Stanford University, 3 plates, 179 p.

Gans, P.B., 1987, An open-system, two-layer crustal stretching model for the eastern Great Basin: Tectonics, v. 6, p. 1–12, https://doi.org/10.1029/TC006i001p00001.

Gans, P.B., and Miller, E.L., 1983, Style of mid-Tertiary extension in east-central Nevada, *in* Gurgel, K.D., ed., Geologic Excursions in the Overthrust Belt and Metamorphic Core Complexes of the Intermountain Region: Utah Geological and Mineral Survey Special Studies 59, p. 107–160.

Gans, P.B., Miller, E.L., McCarthy, J., and Oldcott, M.L., 1985, Tertiary extensional faulting and evolving ductile-brittle transition zones in the northern Snake Range and vicinity: New insights from seismic data: Geology, v. 13, p. 189–193, https://doi.org/10.1130/0091-7613(1985)13<189:TEFAED>2.0.CO;2.

Gans, P.B., Mahood, G.A., and Schermer, E., 1989, Synextensional Magmatism in the Basin and Range Province: A Case Study from the Eastern Great Basin: Geological Society of America Special Paper 223, 53 p., https://doi.org/10.1130/SPE233-p1.

Gans, P.B., Seedorff, E., Fahey, P.L., Hasler, R.W., Maher, D.J., Jeanne, R.A., and Shaver, S.A., 2001, Rapid Eocene extension in the Robinson district, White Pine County, Nevada: Constraints for $^{40}Ar/^{39}Ar$ dating: Geology, v. 29, p. 475–487, https://doi.org/10.1130/0091-7613(2001)029<0475:REEITR>2.0.CO;2.

Gébelin, A., Mulch, A., Teyssier, C., Heizler, M., Vennemann, T., and Seaton, N.C.A., 2011, Oligo-Miocene extensional tectonics and fluid flow across the northern Snake Range detachment system, Nevada: Tectonics, v. 30, TC5010, https://doi.org/10.1029/2010TC002797.

Greene, D.C., 2014, The Confusion Range, west-central Utah: Fold-thrust deformation and a western Utah thrust belt in the Sevier hinterland: Geosphere, v. 10, p. 148–169, https://doi.org/10.1130/GES00972.1.

Hagstrum, J.T., and Gans, P.B., 1989, Paleomagnetism of the Oligocene Kalamazoo Tuff: Implications for Middle Tertiary extension in east-central Nevada: Journal of Geophysical Research, v. 94, p. 1827–1842, https://doi.org/10.1029/JB094iB02p01827.

Harry, D.L., Sawyer, D.S., and Leeman, W.F., 1993, The mechanics of continental extension in western North America: Implications for the magmatic and structural evolution of the Great Basin: Earth and Planetary Science Letters, v. 117, p. 59–71, https://doi.org/10.1016/0012-821X(93)90117-R.

Hazzard, J.C., and Turner, F.E., 1957, Decollement-type overthrusting in south-central Idaho, northwest Utah, and northeast Nevada [abs.]: Geological Society of America Bulletin, v. 68, p. 1829.

Hazzard, J.C., Misch, P., Wiese, J.H., and Bishop, W., 1953, Large-scale thrusting in northern Snake Range, White Pine County, northeastern Nevada [abs.]: Geological Society of America Bulletin, v. 64, p. 1507.

Henry, C.D., McGrew, A.J., Colgan, J.P., Snoke, A.W., and Brueseke, M.E., 2011, Timing, distribution, amount, and style of Cenozoic extension in the northern Great Basin, *in* Lee, J., and Evans, J.P., eds., Geologic Field Trips to the Basin and Range, Rocky Mountains, Snake River Plain, and Terranes of the U.S. Cordillera: Geological Society of America Field Guide 21, p. 27–66, https://doi.org/10.1130/2011.0021(02).

Hoiland, C.W., 2019, Extracting Tectonic Histories from Metamorphic Rocks in Mountain Belts: Insights from the Snake Range Metamorphic Core Complex, Nevada, and the Brooks Range, Alaska [Ph.D. dissertation]: Palo Alto, California, Stanford University, 388 p.

Hose, R.K., and Blake, M.C., Jr., 1976, Geologic map of White Pine County, Nevada, *in* Geology and Mineral Resources of White Pine County, Nevada: Nevada Bureau of Mines and Geology Bulletin 85, scale 1:250,000, 32 p.

Humphreys, E.D., 1995, Post-Laramide removal of the Farallon slab, western United States: Geology, v. 23, p. 987–990, https://doi.org/10.1130/0091-7613(1995)023<0987:PLROTF>2.3.CO;2.

Jackson, J., and McKenzie, D., 1983, The geometrical evolution of normal fault systems: Journal of Structural Geology, v. 5, p. 471–482, https://doi.org/10.1016/0191-8141(83)90053-6.
Johnston, S.M., 2000, Normal Faulting in the Upper Plate of a Metamorphic Core Complex, Northern Snake Range, Nevada [M.S. thesis]: Palo Alto, California, Stanford University, 60 p.
Kellogg, H.E., 1963, Paleozoic stratigraphy of the southern Egan Range, Nevada: Geological Society of America Bulletin, v. 74, p. 685–708, https://doi.org/10.1130/0016-7606(1963)74[685:PSOTSE]2.0.CO;2.
Lee, J., 1995, Rapid uplift and rotation of mylonitic rocks from beneath a detachment fault: Insights from potassium feldspar $^{40}Ar/^{39}Ar$ thermochronology, northern Snake Range, Nevada: Tectonics, v. 14, p. 54–77, https://doi.org/10.1029/94TC01508.
Lee, J., and Sutter, J.F., 1991, Incremental $^{40}Ar/^{39}Ar$ thermochronology of mylonitic rocks from the northern Snake Range, Nevada: Tectonics, v. 10, p. 77–100, https://doi.org/10.1029/90TC01931.
Lee, J., Miller, E.L., and Sutter, J.F., 1987, Ductile strain and metamorphism in an extensional tectonic setting: A case study from the northern Snake Range, Nevada, U.S.A., *in* Coward, M.P., Dewey, J.F., and Hancock, P.L., eds., Continental Extensional Tectonics: Geological Society [London] Special Publication 28, p. 267–298, https://doi.org/10.1144/GSL.SP.1987.028.01.18.
Lee, J., Miller, E.L., Gans, P.B., and Huggins, C.C., 1999a, Geologic Map of the Mount Moriah Quadrangle, Nevada: Nevada Bureau of Mines and Geology Field Studies Map 19, scale 1:24,000, 1 plate, 12 p.
Lee, J., Gans, P.B., and Miller, E.L., 1999b, Geologic Map of the Third Butte East Quadrangle, Nevada: Nevada Bureau of Mines and Geology Field Studies Map 16, scale 1:24,000, 1 plate, 12 p.
Lee, J., Blackburn, T., and Johnston, S., 2017, Timing of mid-crustal ductile extension in the northern Snake Range metamorphic core complex, Nevada: Evidence from U/Pb zircon ages: Geosphere, v. 13, p. 439–459, https://doi.org/10.1130/GES01429.1.
Lewis, C.J., Wernicke, B.P., Selverstone, J., and Bartley, J.M., 1999, Deep burial of the footwall of the northern Snake Range décollement, Nevada: Geological Society of America Bulletin, v. 111, p. 39–51, https://doi.org/10.1130/0016-7606(1999)111<0039:DBOTFO>2.3.CO;2.
Lister, G.S., and Davis, G.A., 1989, The origin of metamorphic core complexes and detachment faults during Tertiary continental extension in the northern Colorado River region, U.S.A.: Journal of Structural Geology, v. 11, p. 65–94, https://doi.org/10.1016/0191-8141(89)90036-9.
Lister, G.S., Etheridge, M.A., and Symonds, P.A., 1986, Detachment faulting and the evolution of passive continental margins: Geology, v. 14, p. 246–250, https://doi.org/10.1130/0091-7613(1986)14<246:DFATEO>2.0.CO;2.
Long, S.P., 2012, Magnitudes and spatial patterns of erosional exhumation in the Sevier hinterland, eastern Nevada and western Utah, USA: Insights from a Paleogene paleogeologic map: Geosphere, v. 8, p. 881–901, https://doi.org/10.1130/GES00783.1.
Long, S.P., 2015, An upper-crustal fold province in the hinterland of the Sevier orogenic belt, eastern Nevada, U.S.A.: A Cordilleran Valley and Ridge in the Basin and Range: Geosphere, v. 11, p. 404–424, https://doi.org/10.1130/GES01102.1.
Long, S.P., 2019, Geometry and magnitude of extension in the Basin and Range Province (39°N), California, Nevada, and Utah, U.S.A.: Constraints from a province-scale cross section: Geological Society of America Bulletin, v. 131, p. 99–119, https://doi.org/10.1130/B31974.1.
Long, S.P., and Soignard, E., 2016, Shallow-crustal metamorphism during Late Cretaceous anatexis in the Sevier hinterland plateau: Peak temperature conditions from the Grant Range, eastern Nevada, U.S.A.: Lithosphere, v. 8, p. 150–164, https://doi.org/10.1130/L501.1.
Long, S.P., and Walker, J.P., 2015, Geometry and kinematics of the Grant Range brittle detachment system, eastern Nevada, U.S.A.: An end-member style of upper-crustal extension: Tectonics, v. 34, p. 1837–1862, https://doi.org/10.1002/2015TC003918.
Long, S.P., Heizler, M.T., Thomson, S.N., Reiners, P.W., and Fryxell, J.E., 2018, Rapid Oligocene to early Miocene extension along the Grant Range detachment system, eastern Nevada, U.S.A.: Insights from multi-part cooling histories of footwall rocks: Tectonics, v. 37, p. 4752–4779, https://doi.org/10.1029/2018TC005073.
Lund, K., Beard, S.L., and Perry, W.J., 1993, Relation between extensional geometry of the northern Grant Range and oil occurrences in Railroad Valley, east-central Nevada: American Association of Petroleum Geologists Bulletin, v. 77, p. 945–962, https://doi.org/10.1306/BDFF8DA8-1718-11D7-8645000102C1865D.
Martinez, C.M., Miller, E.L., and Stockli, D.F., 1998, Miocene age rock avalanche deposits of the Sacramento Pass Basin, Basin and Range Province, Nevada: Geological Society of America Abstracts with Programs, v. 30, no. 5, p. 53.
Miller, E.L., and Gans, P.B., 1989, Cretaceous crustal structure and metamorphism in the hinterland of the Sevier thrust belt, western U.S. Cordillera: Geology, v. 17, p. 59–62, https://doi.org/10.1130/0091-7613(1989)017<0059:CCSAMI>2.3.CO;2.
Miller, E.L., Gans, P.B., and Garing, J., 1983, The Snake Range décollement: An exhumed mid-Tertiary ductile-brittle transition: Tectonics, v. 2, p. 239–263, https://doi.org/10.1029/TC002i003p00239.
Miller, E.L., Gans, P.B., Wright, J.E., and Sutter, J.F., 1988, Metamorphic history of the east central Basin and Range Province: Tectonic setting and relationship to magmatism, *in* Ernst, W.G., ed., Metamorphism and Crustal Evolution, Western United States: Englewood Cliffs, New Jersey, Prentice-Hall, Rubey Volume VII, p. 649–682.
Miller, E.L., Dumitru, T.A., Brown, R.W., and Gans, P.B., 1999a, Rapid Miocene slip on the Snake Range–Deep Creek Range fault system, east-central Nevada: Geological Society of America Bulletin, v. 111, p. 886–905, https://doi.org/10.1130/0016-7606(1999)111<0886:RMSOTS>2.3.CO;2.
Miller, E.L., Gans, P.B., Grier, S.P., Huggins, C.C., and Lee, J., 1999b, Geologic Map of the Old Man's Canyon Quadrangle, Nevada: Nevada Bureau of Mines and Geology Field Studies Map 21, scale 1:24,000, 1 sheet, 12 p.
Misch, P., 1957, Magnitude and interpretation of some thrusts in northeast Nevada [abs.]: Geological Society of America Bulletin, v. 68, p. 1854–1855.
Misch, P., and Hazzard, J.C., 1962, Stratigraphy and metamorphism of late Precambrian rocks of central northeastern Nevada and adjacent Utah: American Association of Petroleum Geologists Bulletin, v. 46, p. 289–343, https://doi.org/10.1306/BC743823-16BE-11D7-8645000102C1865D.
Moores, E.M., Scott, R.B., and Lumsden, W.W., 1968, Tertiary tectonics of the White Pine–Grant Range, east-central Nevada, and some regional implications: Geological Society of America Bulletin, v. 79, p. 1703–1726, https://doi.org/10.1130/0016-7606(1968)79[1703:TTOTWP]2.0.CO;2.
Platt, J.P., Behr, W.M., and Cooper, F.J., 2015, Metamorphic core complexes: Windows into the mechanics and rheology of the crust: Journal of the Geological Society [London], v. 172, p. 9–27, https://doi.org/10.1144/jgs2014-036.
Rodgers, D.W., 1987, Thermal and Structural Evolution of the Southern Deep Creek Range, West Central Utah and East Central Nevada [Ph.D. dissertation]: Palo Alto, California, Stanford University, 5 plates, 149 p.
Smith, M.E., Carroll, A.R., Jicha, B.R., Cassel, E.J., and Scott, J.J., 2014, Paleogeographic record of Eocene Farallon slab rollback beneath western North America: Geology, v. 42, p. 1039–1042, https://doi.org/10.1130/G36025.1.
Snell, K.E., Koch, P.L., Druschke, P., Foreman, B.Z., and Eiler, J.M., 2014, High elevation of the 'Nevadaplano' during the Late Cretaceous: Earth and Planetary Science Letters, v. 386, p. 52–63, https://doi.org/10.1016/j.epsl.2013.10.046.
Sonder, L.J., and Jones, C.H., 1999, Western United States extension: How the West was widened: Annual Review of Earth and Planetary Sciences, v. 27, p. 417–462, https://doi.org/10.1146/annurev.earth.27.1.417.
Steely, A.N., Janecke, S.U., Long, S.P., Carney, S.J., Oaks, R.Q., Langenheim, V.E., and Link, P.K., 2005, Evolution of a late Cenozoic supradetachment basin above a flat-on-flat detachment with a folded lateral ramp, SE Idaho, *in* Pederson, J., and Dehler, C.M., eds., Interior Western United States: Geological Society of America Field Guide 6, p. 169–198, https://doi.org/10.1130/2005.fld006(08).
Stewart, J.H., 1980, Geology of Nevada: A Discussion to Accompany the Geologic Map of Nevada: Nevada Bureau of Mines and Geology Special Publication 4, 136 p.
Stewart, J.H., and Poole, F.G., 1974, Lower Paleozoic and uppermost Precambrian Cordilleran miogeocline, Great Basin, western United States, *in* Dickinson, W.R., ed., Tectonics and Sedimentation: Society of Economic Paleontologists and Mineralogists (SEPM) Special Publication 22, p. 28–57, https://doi.org/10.2110/pec.74.22.0028.
Suppe, J., 1983, Geometry and kinematics of fault-bend folding: American Journal of Science, v. 283, p. 684–721, https://doi.org/10.2475/ajs.283.7.684.
Taylor, W.J., 1990, Spatial and temporal relations of Cenozoic volcanism and extension in the North Pahroc and Seaman Ranges, eastern Nevada, *in* Wernicke, B.P., ed., Basin and Range Extensional Tectonics near the Latitude of Las Vegas: Geological Society of America Memoir 176, p. 181–193, https://doi.org/10.1130/MEM176-p181.
Taylor, W.J., and Bartley, J.M., 1992, Prevolcanic extensional Seaman breakaway fault and its geologic implications for eastern Nevada and western Utah: Geological Society of America Bulletin, v. 104, p. 255–266, https://doi.org/10.1130/0016-7606(1992)104<0255:PESBFA>2.3.CO;2.
Taylor, W.J., Bartley, J.M., Lux, D.R., and Axen, G.J., 1989, Timing of Tertiary extension in the Railroad Valley–Pioche transect, Nevada: Constraints from $^{40}Ar/^{39}Ar$ ages of volcanic rocks: Journal of Geophysical Research, v. 94, p. 7757–7774, https://doi.org/10.1029/JB094iB06p07757.
Walker, C.T., Francis, R.D., Dennis, J.G., and Lumsden, W.W., 1992, Cenozoic attenuation detachment faulting: A possible control on oil and gas accumulation in east-central Nevada: American Association of Petroleum Geologists Bulletin, v. 76, p. 1665–1686, https://doi.org/10.1306/BDFF8A9C-1718-11D7-8645000102C1865D.

Wells, M.L., and Hoisch, T.D., 2008, The role of mantle delamination in widespread Late Cretaceous extension and magmatism in the Cordilleran orogen, western United States: Geological Society of America Bulletin, v. 120, p. 515–530, https://doi.org/10.1130/B26006.1.

Wernicke, B., 1981, Low-angle normal faults in the Basin and Range Province: Nappe tectonics in an extending orogen: Nature, v. 291, p. 645–648, https://doi.org/10.1038/291645a0.

Wernicke, B., and Burchfiel, B.C., 1982, Modes of extensional tectonics: Journal of Structural Geology, v. 4, p. 105–115, https://doi.org/10.1016/0191-8141(82)90021-9.

Westaway, R., 1999, The mechanical feasibility of low-angle normal faulting: Tectonophysics, v. 308, p. 407–443, https://doi.org/10.1016/S0040-1951(99)00148-1.

Whitney, D.L., Teyssier, C., Rey, P., and Buck, R.W., 2013, Continental and oceanic core complexes: Geological Society of America Bulletin, v. 125, p. 273–298, https://doi.org/10.1130/B30754.1.

Wrobel, A.J., Gans, P.B., and Womer, J.B., 2021, Late Cretaceous crustal shortening in the northern Snake Range metamorphic core complex: Constraints on the structural geometry and magnitude of pre-extensional footwall burial: Tectonics, v. 40, https://doi.org/10.1029/2020TC006460.

Yin, A., 1989, Origin of regional rooted low-angle normal faults: A mechanical model and its implications: Tectonics, v. 8, p. 469–482, https://doi.org/10.1029/TC008i003p00469.

Yin, A., and Dunn, J.F., 1992, Structural and stratigraphic development of the Whipple-Chemehuevi detachment fault system, southeastern California: Implications for the geometrical evolution of domal and basinal low-angle normal faults: Geological Society of America Bulletin, v. 104, p. 659–674, https://doi.org/10.1130/0016-7606(1992)104<0659:SASDOT>2.3.CO;2.

Yonkee, W.A., and Weil, A.B., 2015, Tectonic evolution of the Sevier and Laramide belts within the North American Cordillera orogenic system: Earth-Science Reviews, v. 150, p. 531–593, https://doi.org/10.1016/j.earscirev.2015.08.001.

Young, J.C., 1960, Structure and Stratigraphy in the North-Central Schell Creek Range, Eastern Nevada [Ph.D. dissertation]: Princeton, New Jersey, Princeton University, 207 p., 3 plates.

Zuza, A.V., Thorman, C., Henry, C., Levy, D., Dee, S., Long, S., Sandberg, C., and Soignard, E., 2020, Pulsed Mesozoic deformation in the Cordilleran hinterland and evolution of the Nevadaplano: Insights from the Pequop Mountains, NE Nevada: Lithosphere, v. 2020, https://doi.org/10.2113/2020/8850336.

Zuza, A.V., Levy, D.A., and Mulligan, S., 2022, Geologic field evidence for non-lithostatic overpressure recorded in the North American Cordillera hinterland, northeast Nevada: Geoscience Frontiers, v. 13, https://doi.org/10.1016/j.gsf.2020.10.006.